Available online at www.sciencedirect.com
SCIENCE DIRECT®
Journal of Computational Physics 193 (2004) 563–594
JOURNAL OF COMPUTATIONAL PHYSICS
www.elsevier.com/locate/jcp

High order one-step monotonicity-preserving schemes for unsteady compressible flow calculations

V. Daru [a,b], C. Tenaud [b,*]

[a] ENSAM, 151 Boulevard de l'Hôpital, 75013 Paris, France
[b] LIMSI – CNRS, B.P. 133, Campus d'Orsay, F-91403 Orsay Cedex, France

Received 12 November 2002; received in revised form 12 August 2003; accepted 14 August 2003

Abstract

This paper deals with the development of accurate one-step schemes for the numerical simulation of unsteady compressible flows. Pursuing our work in Daru and Tenaud [V. Daru, C. Tenaud, Comput. Fluids 30 (2001) 89] where third-order schemes were considered, we follow the Lax–Wendroff approach to develop high order TVD combined time–space schemes by correcting the successive modified equations. In the scalar case, TVD schemes accurate up to seventh order (OSTVD7) in time and space are obtained (in smooth regions and away from extrema). To avoid the clipping and the loss of accuracy that is common to the TVD schemes near extrema, we develop monotonicity-preserving (MP) conditions derived from Suresh and Huynh [A. Suresh, H.T. Huynh, J. Comput. Phys. 136 (1997) 83] to locally relax the TVD limitation for this family of one-step schemes. Numerical results for long time integration in the scalar case show that the MP one-step approach gives the best results compared to several multistage schemes, including WENO schemes. The extension to systems and to the multidimensional case is done in a simplified way which does not preserve the scalar order of accuracy. However we show that the resulting schemes have a very low level of error. For validation, the present algorithm has been checked on several classical one-dimensional and multidimensional test cases, including both viscous and inviscid flows: a moving shock wave interacting with a sine wave, the Lax shock tube problem, the 2D inviscid double Mach reflection and the 2D viscous shock wave–vortex interaction. By computing these various test cases, we demonstrate that very accurate results can be obtained by using the one-step MP approach which is very competitive compared to multistage high order schemes.

Keywords: High order scheme; Unsteady flows; Compressible flows; Shock capturing scheme

1. Introduction

In the high speed flow regime, many aerodynamic configurations involve interactions between shock waves and turbulence such as, for instance, within air intakes where shock wave-turbulent boundary

* Corresponding author. Tel.: +33-1-6985-8130; fax: +33-1-6985-8088.
E-mail address: tenaud@limsi.fr (C. Tenaud).

0021-9991/$ - see front matter © 2003 Elsevier B.V. All rights reserved.
doi:10.1016/j.jcp.2003.08.023

layer or shock wave-shear layer interactions occur. An accurate prediction of such interactions is of importance in effective design of supersonic vehicles since they greatly affect the aerodynamic loads. At the present time, it is commonly admitted that large Eddy simulation (LES) is a highly promising technique for the prediction of complex shock wave turbulence interactions including large-scale flow phenomena such as those encountered in engineering applications [8,12]. Recent CFD predictions of shock wave turbulent boundary layer interactions is summarized in [12]. A review of the LES of compressible flows can also be found in [16]. It is well known that, in the LES approach, the numerical scheme must have low dissipation to minimize the interaction with the subgrid scale model. In the past, high order accurate schemes, like spectral ([3,4,18]) or Padé schemes ([14,17]), have been identified as suitable tools for LES. Nevertheless, in the transonic and supersonic flow regimes when dealing with flows involving shock waves, one must use a numerical scheme which can both represent small scale structures with the minimum of numerical dissipation, and capture discontinuities with the robustness that is common to Godunov-type methods. To achieve this dual objective, high order accurate shock capturing schemes must be employed. However, as pointed out by Titarev and Toro [26], the design of high order accurate numerical schemes for hyperbolic conservation laws is a formidable task since three major difficulties have to be overcome: ensuring the conservation property, preserving the high order of accuracy in both time and space and controlling the generation of the spurious oscillations in the vicinity of discontinuities.

At present, the numerical methods generally employed can basically be divided into two approaches: a coupled time and space (one-step) approach and separate time and space integrations. On the one hand, the methods for which time and space are considered separately, are generally based on a multistage time integration. The most recent highly accurate separate time–space methods use a Runge–Kutta type time discretization. In each stage of the time integration, a high order spatial discretization equipped with a shock capturing technique is applied ensuring non-oscillatory and conservation properties. As the spatial support of the high order reconstruction is relatively large, the global stencil of a decoupled time–space scheme is much larger than that of a coupled time–space approach for the same order of accuracy since the space discretization is applied in each sub-step of the time integration. Following that approach, one does not control the total truncation error of the scheme and the limiting process acts only on the space discretization while the time integration stays invariant. Moreover, it is not possible to reach very high order of accuracy in time without introducing spurious oscillations. For instance, using a Runge–Kutta method, the TVD property cannot be recovered for an accuracy greater than fifth order. To recover the TVD property for the fourth and fifth order, one needs to solve adjoint problems during the sub-steps, which is very expensive. On the other hand, the coupled time and space schemes are preferably developed on a Lax–Wendroff type approach. The schemes constructed in this way use a minimum stencil. As will be shown, this approach is also very attractive for controlling the total truncation error (at least in the scalar case), and deriving optimal non-oscillatory conditions. However the extension to non-linear systems of equations is not trivial, and the integration of source terms is delicate.

Whatever the approach (coupled or decoupled), an ad hoc discontinuity-capturing feature must be employed to limit the spurious oscillations in the vicinity of the strong gradient regions. Among the shock capturing techniques found in the literature, total variation diminishing (TVD) schemes are generally considered to be well suited for the capture of shock waves but too diffusive in smooth regions, due to the limitation of the accuracy to first order near extrema. More recent schemes like the ENO/WENO [10,20–23] family are very accurate in smooth regions but show a diffusive behavior in the vicinity of discontinuities. Also, these schemes are very expensive in terms of CPU time (for example the high order WENO schemes turns out to be too costly to be used for grid convergence studies in several cases reported in [24]). A WENO reconstruction was also used recently in the ADER approach by Titarev and Toro [26], together with a coupled time–space integration. However, it is likely that the scheme might suffer from the same drawbacks as the WENO schemes.

Another successful approach has recently been developed in [25] to enlarge the TVD constraint for a better representation near extrema. The development has been performed on a separate time and space integration by using a high order polynomial fixed stencil reconstruction and Runge–Kutta time stepping. The reconstructed values at the interfaces of the mesh cells are then limited such as to preserve both monotonicity and high order accuracy. This is achieved by using local geometrical considerations to relax the monotonicity constraints near extrema. This limiting strategy has then been extended to the WENO family of schemes in [2], in order to avoid the oscillations which sometimes can develop with high order WENO reconstructions. However, in some sense this negates the key ingredient of the WENO schemes, which is the use of a variable stencil to obtain a non-oscillatory reconstruction.

In this paper, our aim is to show that, contrary to the commonly admitted opinion, very accurate and efficient one-step schemes can be developed in the TVD framework. We retain the coupled time and space approach and a fixed stencil to develop highly accurate numerical schemes that can be rendered TVD or monotonicity preserving with control over the total truncation error. Being one-step, these schemes are very efficient. Pursuing our work in [7] where third-order schemes were considered, we obtain higher order schemes by correcting the error terms at the desired order in the equivalent equation. The implementation of these schemes is very simple as the increase of accuracy can be obtained via a change of an ''accuracy function'' applied to a classical second-order scheme. The schemes can then recover the TVD property by applying a limitation on this specific function. In the scalar case, TVD schemes accurate up to the seventh order in time and space are obtained in smooth regions and away from extrema. These schemes have however a tendency to clip extrema, a drawback which is inherent in all TVD schemes. By highlighting the geometric significance of the TVD constraints, we develop monotonicity-preserving (MP) conditions derived from [25] to relax the TVD limitation near extrema for this family of one-step schemes. We thus obtain very accurate non-oscillatory results. Comparisons are made in the scalar case with the Runge–Kutta scheme developed in [25], which turn out in favor of the one-step approach. The latter has better control over the total dissipation of the scheme, while a multistage approach controls only the spatial dissipation. Moreover, the cost (in terms of CPU time) of the one-step scheme is much lower. In the 1D scalar case, it appears that our one-step schemes are very similar to those proposed by Leonard [15] for solving the advection equation, although the formulation and the method of construction are quite different (Leonard uses high order characteristic interpolations). To our knowledge, this study has however remained restricted to the 1D linear scalar case, and was not extended to flow computations. We also believe that the TVD formulation that we use here is better adapted for generalizations to the case of non-linear systems. Though the extensions to systems of equations and to multidimensions are not trivial when using a coupled time and space integration, we propose an extension of the present scheme to the Euler and Navier–Stokes equations, based on the classical Roe flux difference splitting and dimensional splitting. The resulting schemes are only second-order accurate, but they are very economical in terms of CPU time and their level of error is very low as shown by convergence studies, making them attractive for use in cases where it is not possible to use very fine meshes (for example in LES calculations where all the length scales are not fully resolved).

This study is limited to uniform cartesian meshes. The extension of the one-step schemes to general curvilinear meshes can be done using a classical coordinate transformation. If the transformation is not sufficiently smooth, the good properties of the schemes can of course deteriorate, but this is a problem common to all approaches (for example the high order finite difference ENO/WENO schemes can apply only to uniform or smoothly varying grids; multidimensional finite volume schemes do not share this drawback but are very complicated and costly, see [5,23]). The dimensional splitting we use in the multidimensional case is not applicable to unstructured meshes. This is indeed a disadvantage, but structured meshes are still widely used for CFD studies.

The paper is organized as follows: in Section 2, we consider the scalar case. We construct the one-step high order schemes, and derive the TVD and MP versions of these schemes. The multistage approach is also

presented in the TVD context for comparison. We then extend the one-step scheme to the Euler and Navier–Stokes equations in Section 3. In Section 4 convergence studies and numerical results for various 1D and 2D test cases are presented, demonstrating that very accurate results can be obtained by using the one-step MP approach.

2. High order schemes: the scalar case

To present the numerical schemes we developed in this study, we first focus on the solution $u(x,t)$ of the linear scalar transport equation

$$u_t + f(u)_x = 0 \tag{1}$$

with $f(u) = au$, a being the velocity which is supposed to be constant. For simplicity, we will suppose in the following that $a > 0$. The case $a < 0$ can however be treated by symmetry relative to each cell interface. In view of the discretization of this equation, we will denote by δt and δx the time step and cell width, respectively. u_j^n will denote the numerical solution at time $t = t_0 + n \cdot \delta t$ and position $x = x_0 + j \cdot \delta x$.

In the following, we present the development of the coupled time–space one-step schemes. In order to draw a parallel with the one-step scheme and to also highlight the differences, the separate space-time discretization will also be presented though this is a classical approach.

2.1. Development of high order one-step schemes

2.1.1. Unlimited schemes

The one-step approach is of the Lax–Wendroff type [13], i.e., the time Taylor series expansion is used to express u_j^{n+1} and the time derivatives are substituted with space derivatives using the exact equation. The construction of such schemes can equivalently be obtained by correcting the successive error terms of the modified equations to increase the order of accuracy of the schemes. In this way, we obtain high order accurate schemes relative to both time and space. To begin, let us consider the Lax–Wendroff scheme:

$$u_j^{n+1} = u_j^n - \frac{\delta t}{\delta x}(F_{j+1/2}^{lw} - F_{j-1/2}^{lw}), \tag{2}$$

where $F_{j+1/2}^{lw}$ is the numerical flux:

$$F_{j+1/2}^{lw} = f_j^n + \frac{(1-v)}{2}(f_{j+1}^n - f_j^n) \tag{3}$$

and v is the CFL number $v = a(\delta t/\delta x)$. The modified equation for this scheme reads:

$$u_t + f(u)_x = a\frac{\delta x^2}{6}(v^2 - 1)u_{xxx}. \tag{4}$$

By subtracting from the Lax–Wendroff scheme an upwind term formed by discretizing the right-hand side of (4), one obtains the classical third-order upwind-biased scheme with a numerical flux which can be written:

$$F_{j+1/2}^3 = f_j^n + \frac{(1-v)}{2}\left(f_{j+1}^n - f_j^n - \frac{1+v}{3}(f_{j+1}^n - 2f_j^n + f_{j-1}^n)\right). \tag{5}$$

For convenience, this numerical flux can be recast in the following form:

$$F_{j+1/2}^3 = f_j^n + \Phi_{j+1/2}^3\frac{(1-v)}{2}(f_{j+1}^n - f_j^n) \tag{6}$$

with

$$\Phi^3_{j+1/2} = 1 - \frac{1+v}{3}(1 - r_{j+1/2}) \tag{7}$$

and $r_{j+1/2} = (u^n_j - u^n_{j-1})/(u^n_{j+1} - u^n_j)$. Thus, the third-order scheme is expressed in the usual form of a second-order flux limiter scheme, and the Φ function plays the role of an accuracy function.

Following such successive corrections of the higher order error terms, one can construct schemes of arbitrarily high o-th order of accuracy, whose numerical flux can be written in the generic form

$$F^o_{j+1/2} = f^n_j + \Phi^o_{j+1/2}\frac{(1-v)}{2}(f^n_{j+1} - f^n_j) \tag{8}$$

depending only on the function $\Phi^o_{j+1/2}$ which drives the o-th order of accuracy of the scheme.

For example, to construct the function Φ^4, we derive the modified equation of the third-order scheme, which reads:

$$u_t + f(u)_x = a\frac{\delta x^3}{24}(v^2 - 1)(2 - v)u_{xxxx} \tag{9}$$

and substract from the scheme a term formed by discretizing the RHS of (9). In this way we obtain the function Φ^4 corresponding to a fourth-order (in time and space) scheme:

$$\Phi^4_{j+1/2} = \Phi^3_{j+1/2} + \frac{1+v}{3}\cdot\frac{v-2}{4}(1 - 2\ r_{j+1/2} + r_{j+1/2}\ r_{j-1/2}). \tag{10}$$

We have performed the successive derivations of the modified equations up to sixth order. We only give here the functions Φ^5, Φ^6 and Φ^7 corresponding to the fifth-, sixth- and seventh-order numerical schemes obtained by correcting these modified equations:

$$\begin{aligned}
\Phi^5_{j+1/2} &= \Phi^4_{j+1/2} - \frac{1+v}{3}\cdot\frac{v-2}{4}\cdot\frac{v-3}{5}\cdot\left(\frac{1}{r_{j+3/2}} - 3 + 3\ r_{j+1/2} - r_{j+1/2}\ r_{j-1/2}\right),\\
\Phi^6_{j+1/2} &= \Phi^5_{j+1/2} + \frac{1+v}{3}\cdot\frac{v-2}{4}\cdot\frac{v-3}{5}\cdot\frac{v+2}{6}\\
&\quad\cdot\left(\frac{1}{r_{j+3/2}\ r_{j+5/2}} - \frac{4}{r_{j+3/2}} + 6 - 4\ r_{j+1/2} + r_{j+1/2}\ r_{j-1/2}\right),\\
\Phi^7_{j+1/2} &= \Phi^6_{j+1/2} - \frac{1+v}{3}\cdot\frac{v-2}{4}\cdot\frac{v-3}{5}\cdot\frac{v+2}{6}\cdot\frac{v+3}{7}\\
&\quad\cdot\left(\frac{1}{r_{j+3/2}\ r_{j+5/2}} - \frac{5}{r_{j+3/2}} + 10 - 10\ r_{j+1/2} + 5\ r_{j+1/2}\ r_{j-1/2} - r_{j+1/2}\ r_{j-1/2}\ r_{j-3/2}\right).
\end{aligned} \tag{11}$$

Let us emphasize that the numerical schemes constructed in this way always have the same order of accuracy in time and space. The most interesting functions are the odd ones because they correspond to schemes having a dominant dissipative error (even derivative in the right-hand side of the modified equation). The dispersive error being one-order lower, the corresponding schemes have a nearly symmetric behavior.

Comparing the stencil of this scheme to the Runge–Kutta high order scheme described in the following (Section 2.1.6), here we use a stencil of only eight points to get a seventh-order scheme relative to both time and space. Also notice that this kind of scheme has the property, which seems desirable, of giving the exact solution if the CFL number is equal to 1 (the schemes have a classical CFL stability condition $0 \leqslant v \leqslant 1$).

2.1.2. TVD schemes

The general constraint for a one-step scheme to be TVD, following the criteria developed by Harten, is:

$$-\frac{2}{v} \leqslant \Phi_{j-1/2} - \Phi_{j+1/2}/r_{j+1/2} \leqslant \frac{2}{1-v}. \tag{12}$$

If, as usual, Φ is set to zero for negative values of r, this leads to:

$$\begin{cases} 0 \leqslant \Phi_{j+1/2} \leqslant \dfrac{2}{1-v}, \\ 0 \leqslant \Phi_{j+1/2} \leqslant \dfrac{2r_{j+1/2}}{v}. \end{cases} \tag{13}$$

The upper bound of these limits is

$$\max\left(0, \min\left(\frac{2}{1-v}, \Phi_{j+1/2}, \frac{2\ r_{j+1/2}}{v}\right)\right).$$

The most usual limiters use the most restrictive of these values under a CFL condition $0 \leqslant v \leqslant 1$, that is:

$$\begin{cases} 0 \leqslant \Phi_{j+1/2} \leqslant 2, \\ 0 \leqslant \Phi_{j+1/2} \leqslant 2\ r_{j+1/2}. \end{cases} \tag{14}$$

In fact, there is no real necessity to restrict the constraints except in the case where a steady solution is searched, which should be independent of the CFL number. In the general unsteady case, it is worth keeping the original constraints. In such a way, it is possible to construct higher than second-order TVD schemes. In [1], such a third-order TVD scheme was proposed. The limiter function was

$$\Phi^{3\text{-TVD}} = \max\left(0, \min\left(\frac{2}{1-v}, \Phi^3, \frac{2\ r_{j+1/2}}{v}\right)\right). \tag{15}$$

This limiter was also used in [7] to compute a viscous flow in a shock tube.

The principle can naturally be extended to higher order schemes, using the Φ function described above. As a general rule, a o-th order TVD scheme will be obtained by taking Φ as $\Phi^{o\text{-TVD}}$, where

$$\Phi^{o\text{-TVD}} = \max\left(0, \min\left(\frac{2}{1-v}, \Phi^o, \frac{2\ r_{j+1/2}}{v}\right)\right). \tag{16}$$

The resulting scheme will be o-th order accurate almost everywhere, except around extrema and discontinuities where it becomes first-order accurate, as is the case for all TVD schemes. This is a serious drawback that needs correction for our purpose.

2.1.3. Geometrical interpretation of the TVD conditions

We would like here to introduce an original geometrical interpretation of the TVD conditions previously presented. This will establish the link between TVD schemes and the monotonicity preserving constraints developed in [25]. Let us write the numerical flux of a one-step scheme as:

$$F_{j+1/2} = f_j^n + \Phi_{j+1/2}\frac{(1-v)}{2}(f_{j+1}^n - f_j^n) = f_j^n + \gamma^+(f_{j+1}^n - f_j^n) \tag{17}$$

with

$$\gamma^+ = \Phi_{j+1/2}\frac{(1-v)}{2}. \tag{18}$$

The first TVD constraint $0 \leqslant \Phi_{j+1/2} \leqslant 2/(1-v)$ is equivalent to $0 \leqslant \gamma^{+} \leqslant 1$, so this amounts to saying that the numerical flux $F_{j+1/2}$ must belong to the interval $[f_j^n, f_{j+1}^n]$.

In regard to the second TVD constraint, let us now introduce the numerical flux defining an upper limit:

$$f_j^{\mathrm{ul}} = f_j^n + \frac{1-v}{v}(f_j^n - f_{j-1}^n) \tag{19}$$

and rewrite the flux $F_{j+1/2}$ as:

$$F_{j+1/2} = f_j^n + \Phi_{j+1/2}\frac{v}{2\ r_{j+1/2}}(f_j^{\mathrm{ul}} - f_j^n) = f_j^n + \gamma^{-}(f_j^{\mathrm{ul}} - f_j^n) \tag{20}$$

with

$$\gamma^{-} = \Phi_{j+1/2}\frac{v}{2\ r_{j+1/2}}. \tag{21}$$

The second TVD constraint $0 \leqslant \Phi_{j+1/2} \leqslant (2\ r_{j+1/2})/v$ amounts here to saying that the coefficient γ^{-} must take values in between 0 and 1, i.e. the numerical flux $F_{j+1/2}$ must belong to the interval $[f_j^n, f_j^{\mathrm{ul}}]$.

Finally the TVD conditions can be expressed by enforcing the interface numerical flux value $F_{j+1/2}$ in the intersection of the two intervals $[f_j^n, f_{j+1}^n]$ and $[f_j^n, f_j^{\mathrm{ul}}]$. This shows that the TVD conditions are identical to the first-order geometrical constraints derived in [25] for the multistage case.

2.1.4. Monotonicity-preserving schemes

We now would like to enlarge the intervals defined above in order to avoid the loss of accuracy near extrema that is common to TVD schemes. To recover an accurate value of the numerical flux near an extremum, the TVD constraint should not be activated. To this end, we here adapt the method derived in [25] to be optimum for the one step schemes.

We note by $[f^1, f^2, \ldots, f^k]$ the interval $[\min(f^1, f^2, \ldots, f^k), \max(f^1, f^2, \ldots, f^k)]$. In [25], the first interval $[f_j^n, f_{j+1}^n]$ is enlarged to $[f_j^n, f_{j+1}^n, f_j^{\mathrm{md}}]$, where:

$$f_j^{\mathrm{md}} = \frac{1}{2}(f_j^n + f_{j+1}^n) - \frac{1}{2}d_{j+1/2} \tag{22}$$

and the second interval $[f_j^n, f_j^{\mathrm{ul}}]$ is enlarged to $[f_j^n, f_j^{\mathrm{ul}}, f_j^{\mathrm{lc}}]$ where:

$$f_j^{\mathrm{lc}} = f_j^n + \frac{1}{2}(f_j^n - f_{j-1}^n) + \frac{\beta}{3}d_{j-1/2} \tag{23}$$

with $d_{j+1/2} = d_{j+1/2}^{\mathrm{MM}} = \mathrm{minmod}(d_j, d_{j+1})$ and $d_j = f_{j+1}^n - 2f_j^n + f_{j-1}^n$ is a measurement of the local curvature of the flux function (we work here directly with the fluxes, contrary to [25] where reconstructed values at the interface are used). The coefficient β is a heuristic factor giving freedom for the value of the local curvature.

In order to satisfy the monotonocity preserving criteria, the numerical flux $F_{j+1/2}$ must belong to the intersection of the enlarged intervals $[f_j^n, f_{j+1}^n, f_j^{\mathrm{md}}]$ and $[f_j^n, f_j^{\mathrm{ul}}, f_j^{\mathrm{lc}}]$. This provides room for the numerical flux to maintain an accurate value.

In the context of our TVD flux limiter one step schemes, we follow the same procedure but rather use the following value for f_j^{lc}:

$$f_j^{\mathrm{lc}} = f_j^n + \frac{1}{2}\left(1 + \frac{d_{j-1/2}}{f_j^n - f_{j-1}^n}\right)(f_j^{\mathrm{ul}} - f_j^n) = f_j^n + \gamma_{\mathrm{lc}}^{-}(f_j^{\mathrm{ul}} - f_j^n), \tag{24}$$

where

$$\gamma_{\mathrm{lc}}^{-} = \frac{1}{2}\left(1 + \frac{d_{j-1/2}}{f_j^n - f_{j-1}^n}\right). \tag{25}$$

This choice for f_j^{lc} is more natural as expressed in terms of f_j^{ul}, and also suppresses the need for the coefficient β.

Let us also rewrite f_j^{md} in a similar form:

$$f_j^{\mathrm{md}} = f_j^n + \gamma_{\mathrm{md}}^{+}(f_{j+1}^n - f_j^n), \tag{26}$$

where

$$\gamma_{\mathrm{md}}^{+} = \frac{1}{2}\left(1 - \frac{d_{j+1/2}}{f_{j+1}^n - f_j^n}\right). \tag{27}$$

Now we can see that if $0 \leqslant \gamma_{\mathrm{md}}^{+} \leqslant 1$ and $0 \leqslant \gamma_{\mathrm{lc}}^{-} \leqslant 1$, then f_j^{md} and f_j^{lc} belong to the TVD intervals. Thus the TVD conditions are not modified in this case. The first inequality $0 \leqslant \gamma_{\mathrm{md}}^{+} \leqslant 1$ gives:

$$0 \leqslant \frac{1}{2}\left(1 - \frac{d_{j+1/2}}{f_{j+1}^n - f_j^n}\right) \leqslant 1 \tag{28}$$

or equivalently:

$$\left|\frac{d_{j+1/2}}{f_{j+1}^n - f_j^n}\right| \leqslant 1. \tag{29}$$

The second inequality $0 \leqslant \gamma_{\mathrm{lc}}^{-} \leqslant 1$ gives:

$$0 \leqslant \frac{1}{2}\left(1 + \frac{d_{j-1/2}}{f_j^n - f_{j-1}^n}\right) \leqslant 1 \tag{30}$$

or equivalently:

$$\left|\frac{d_{j-1/2}}{f_j^n - f_{j-1}^n}\right| \leqslant 1. \tag{31}$$

This shows that the two inequalities are identical. Next let us show that the inequality (29) is always verified in the case where the numerical values $f_{j+l}, l \in \{-1, 0, 1, 2\}$ are monotone. Without loss of generality, we can suppose increasing values. If d_j and d_{j+1} have opposite signs, $d_{j+1/2}$ is equal to zero and the conclusion is trivial. Let us suppose that $d_j \geqslant 0$ and $d_{j+1} \geqslant 0$. Eq. (29) can be developed as

$$\min\left(\left|\frac{f_{j+2}^n - f_{j+1}^n}{f_{j+1}^n - f_j^n} - 1\right|, \left|1 - \frac{f_j^n - f_{j-1}^n}{f_{j+1}^n - f_j^n}\right|\right) \leqslant 1. \tag{32}$$

If $d_j \geqslant 0$, then $f_{j+1}^n - f_j^n \geqslant f_j^n - f_{j-1}^n \geqslant 0$, implying that $0 \leqslant 1 - (f_j^n - f_{j-1}^n)/(f_{j+1}^n - f_j^n) \leqslant 1$. The case where $d_j \leqslant 0$ and $d_{j+1} \leqslant 0$ is symmetrical. This shows that (29) is always verified for monotone numerical data. The enlarged intervals being identical to the TVD intervals, the numerical scheme is MP.

To remain in the TVD framework, we also can express the MP conditions that the numerical flux $F_{j+1/2}$ must belong to the intersection of the enlarged intervals $[f_j^n, f_{j+1}^n, f_j^{\mathrm{md}}]$ and $[f_j^n, f_j^{\mathrm{ul}}, f_j^{\mathrm{lc}}]$ directly as constraints on Φ, namely:

$$\min(0, \Phi^{\mathrm{md}}) \leqslant \Phi \leqslant \max\left(\frac{2}{1-v}, \Phi^{\mathrm{md}}\right), \tag{33}$$

where

$$\Phi^{\mathrm{md}}_{j+1/2} = \left(\frac{2}{1-v}\right)\gamma^{+}_{\mathrm{md}} = \frac{2}{1-v}\frac{f^{\mathrm{md}}_j - f^n_j}{f^n_{j+1} - f^n_j} \tag{34}$$

for the first condition, and

$$\min\left(0, \frac{2r}{v}, \Phi^{\mathrm{lc}}\right) \leqslant \Phi \leqslant \max\left(0, \frac{2r}{v}, \Phi^{\mathrm{lc}}\right), \tag{35}$$

where

$$\Phi^{\mathrm{lc}}_{j+1/2} = \left(\frac{2\ r_{j+1/2}}{v}\right)\gamma^{-}_{\mathrm{lc}} = \frac{2\ r_{j+1/2}}{v}\ \frac{f^{\mathrm{lc}}_j - f^n_j}{f^{\mathrm{ul}}_j - f^n_j} \tag{36}$$

for the second condition.

Finally the MP constraint which preserves accuracy takes the form:

$$\Phi^{o\text{-MP}} = \max(\Phi^{\min}, \min(\Phi^o, \Phi^{\max})), \tag{37}$$

where

$$\Phi^{\min} = \max\left(\min(0, \Phi^{\mathrm{md}}), \min\left(0, \frac{2r}{v}, \Phi^{\mathrm{lc}}\right)\right) \tag{38}$$

and

$$\Phi^{\max} = \min\left(\max\left(\frac{2}{1-v}, \Phi^{\mathrm{md}}\right), \max\left(0, \frac{2r}{v}, \Phi^{\mathrm{lc}}\right)\right). \tag{39}$$

In practice, as was done in [25], the criteria is strengthened by choosing a different definition for the curvature measurement $d_{j+1/2}$, namely

$$d_{j+1/2} = d^{\mathrm{M4}}_{j+1/2} = \mathrm{minmod}(4d_j - d_{j+1}, 4d_{j+1} - d_j, d_j, d_{j+1}). \tag{40}$$

This reduces the range of values left to $\Phi^{o\text{-MP}}$ in the case of a non-monotone discontinuity.

To conclude this section, let us remark that MP schemes are close to TVB (Total Variation Bounded) schemes (see [19]) in the sense that the Total Variation of the numerical solution is allowed to increase for an amount $\mathrm{O}(\delta x)$ in both cases. The essential difference is that MP schemes allow this increase only for non-monotone data, and are TVD for monotone data such that the scheme is not oscillatory around discontinuities. In the TVB case, the Total Variation is allowed to increase everywhere, and oscillations can develop whose amplitude is controlled by an heuristic factor.

2.1.5. Extension to the non-linear case

In the non-linear scalar case, the one-step scheme can be extended in order to preserve the high order of accuracy in both time and space, in the case where the flux function f depends only on u. We can show that the Jacobian $a(u) = \mathrm{d}f/\mathrm{d}u$ verifies the same equation as the variable u, that is:

$$a_t + a(u)a_x = 0. \tag{41}$$

This is easily shown by deriving:

$$a_t + a(u)a_x = \frac{\mathrm{d}a}{\mathrm{d}u}(u_t + a(u)u_x) = 0. \tag{42}$$

Following these equations, the time derivatives can then be replaced by the space derivatives in the Lax–Wendroff procedure. For instance, let us write down the first through third derivatives in time by using successive derivatives of the exact equation:

$$\begin{cases} u_t &= -f_x, \\ u_{tt} &= (a\ f_x)_x, \\ u_{ttt} &= (a\ f_x)_{xt} = (a_t\ f_x + a\ f_{tx})_x, \\ &= (a_t\ f_x - a\ (a\ f_x)_x)_x, \\ &= ((a_t + a\ a_x)f_x - (a^2\ f_x)_x)_x, \\ &= -(a^3\ u_x)_{xx}. \end{cases} \tag{43}$$

Similarly, we can show that in general we get for the mth time derivative:

$$u_{mt} = ((-a)^m\ u_x)_{(m-1)x}. \tag{44}$$

Following this relation, the successive modified equation that we established in the linear case takes the general form in the non-linear case:

$$u_t + f(u)_x = \frac{\delta x^{m-1}}{m!}(\omega(v)a(u)u_x)_{(m-1)x}, \tag{45}$$

where $\omega(v)$ is a polynomial function of $v = a(u)\delta t/\delta x$. In this way, the only modification we have to include in the expression of the high order terms is to include $\omega(v)$ in the difference formulae. Let us illustrate the present development on the third order flux (see (5) in the linear case), which then is in the non-linear case written:

$$F^3_{j+1/2} = f^n_j + \frac{(1-v)_{j+1/2}}{2}(f^n_{j+1} - f^n_j) - \left(\frac{(1-v^2)_{j+1/2}}{6}(f^n_{j+1} - f^n_j) - \frac{(1-v^2)_{j-1/2}}{6}(f^n_j - f^n_{j-1})\right). \tag{46}$$

The flux is written for the case where $a(u) > 0$, but it is easily generalized by symmetry. The function $\Phi^3_{j+1/2}$ becomes:

$$\Phi^3_{j+1/2} = 1 - \frac{1}{3}\frac{(1-v^2)_{j+1/2}\left(f^n_{j+1} - f^n_j\right) - (1-v^2)_{j-1/2}\left(f^n_j - f^n_{j-1}\right)}{(1-v)_{j+1/2}\left(f^n_{j+1} - f^n_j\right)} \tag{47}$$

or equivalently:

$$\Phi^3_{j+1/2} = 1 - \frac{1}{3}\frac{(1-v^2)_{j+1/2} - (1-v^2)_{j-1/2}\ r_{j+1/2}}{(1-v)_{j+1/2}}. \tag{48}$$

The present procedure can be pursued to achieve higher order schemes. In this way, the high order accuracy of the schemes can be maintained in both time and space.

Following Harten's general TVD necessary conditions, the TVD constraints should be expressed by:

$$\Phi^{o\text{-TVD}}_{j+1/2} = \max\left(0, \min\left(\frac{2\ r_{j+1/2}}{|\ v_{j+1/2}\ |}\cdot\frac{1-|\ v_{j-1/2}\ |}{1-|\ v_{j+1/2}\ |}, \Phi^o_{j+1/2}, \frac{2}{1-|\ v_{j+1/2}\ |}\right)\right). \tag{49}$$

Note that, in a similar way, the extension of the MP constraint is straightforward.

2.1.6. Multistage TVD and MP schemes

In this approach (the so-called method of lines), the space and time discretizations are performed separately. The most widely used time integration schemes for unsteady computations are Runge–Kutta type ODE solvers. Beside the classical Runge–Kutta solvers, Shu and Osher [22] have derived explicit Runge–Kutta methods up to the fourth order which possess the desirable property of being TVD. Unfortunately, only the second and third-order methods do not necessitate the use of the x-reversed operator (i.e. solving $u_t - f(u)_x = 0$). Their third-order TVD RK3 time integration is widely used. It is written:

$$\begin{cases} u^1 = u^n + \delta t L_{\delta x}(u^n), \\ u^2 = \dfrac{3}{4}u^n + \dfrac{1}{4}u^1 + \dfrac{\delta t}{4}L_{\delta x}(u^1), \\ u^{n+1} = \dfrac{1}{3}u^n + \dfrac{2}{3}u^2 + \dfrac{2}{3}\delta t L_{\delta x}(u^2) \end{cases} \tag{50}$$

with $L_{\delta x}$ being a discrete approximation of $L(u) = -f(u)_x$.

As this specific Runge–Kutta scheme is made up of repeated applications of a single stage scheme given by $u^{k+1} = u^k + \delta t L_{\delta x}(u^k)$, the scheme is completed once $L_{\delta x}$ is chosen. Integrating the single stage scheme over the cell $[x_{j-1/2}, x_{j+1/2}]$, this amounts to approximating the interface value of the flux $f(u^k(x_{j+1/2}))$. Let $F_{j+1/2}$ be the numerical flux approximating this interface flux (the reconstruction step). We will here briefly recall and discuss several different approaches.

The widely used MUSCL reconstruction uses the local slope $\Delta_{j+1/2}$ to express the interface value:

$$F_{j+1/2} = f_j + \frac{1}{2}\Delta_{j+1/2}. \tag{51}$$

Depending on the value given to $\Delta_{j+1/2}$, different schemes can be obtained. A linear combination of $f_{j+1} - f_j$ and $f_j - f_{j-1}$ is classically used, giving a second or third-order space accuracy. To increase the order of accuracy, one can use a larger stencil to express the slope. In [25] for example, the slope $\Delta_{j+1/2}$ is chosen as:

$$\Delta_{j+1/2} = (2f_{j-2} - 13f_{j-1} - 13f_j + 27f_{j+1} - 3f_{j+2})/30, \tag{52}$$

which gives a spatially fifth-order scheme, or:

$$\Delta_{j+1/2} = (-3f_{j-3} + 25f_{j-2} - 101f_{j-1} - 101f_j + 214f_{j+1} - 38f_{j+2} + 4f_{j+3})/210, \tag{53}$$

which gives a spatially seventh-order scheme. The fifth-order scheme uses a six point stencil per Runge–Kutta sub-step, that gives a total stencil of sixteen points per time step. The seventh-order scheme uses an eight point stencil per Runge–Kutta sub-step giving a total stencil of 22 points per time iteration.

Equivalently, as was done in the one-step case, the numerical flux can also be written in the different form:

$$F_{j+1/2} = f_j + \frac{1}{2}\Psi^o_{j+1/2}(f^n_{j+1} - f^n_j), \tag{54}$$

where, for example, the spatially fifth-order scheme corresponds to:

$$\Psi^5_{j+1/2} = \left(2r_{j-1/2}r_{j+1/2} - 11r_{j+1/2} + 24 - \frac{3}{r_{j+3/2}}\right)\Big/30. \tag{55}$$

The slope $\Delta_{j+1/2}$ becomes $\Delta_{j+1/2} = \Psi^o_{j+1/2}(f^n_{j+1} - f^n_j)$, and Ψ is the accuracy function. The above reconstruction methods use a fixed stencil. By contrast, the family of ENO–WENO schemes [10,20–23] is based on the use of a variable stencil to perform the reconstruction, with the idea of selecting the stencil giving the smoothest interpolation.

To recover the TVD property for a multistage scheme, both the Runge–Kutta solver and each space-discretized step of the Runge–Kutta solver are required to be TVD. As the Runge–Kutta scheme is made up of repeated applications of the same single stage scheme, we only have to consider one stage. The corresponding numerical flux was written above as:

$$F_{j+1/2} = f_j + \frac{1}{2}\Psi_{j+1/2}(f^n_{j+1} - f^n_j). \tag{56}$$

The slope must then be limited in order to get a TVD scheme. This can be obtained by applying the TVD constraints on the Ψ function. We obtain:

$$\begin{cases} 0 \leqslant \Psi_{j+1/2} \leqslant 2r_{j+1/2}\dfrac{1-v}{v}, \\ 0 \leqslant \Psi_{j+1/2} \leqslant 2. \end{cases} \tag{57}$$

If one wants to keep the order of accuracy at least equal to 2, it is necessary that $\Psi = 1$ when $r_{j\pm\frac{1}{2}}$ is equal to 1. This implies that the CFL value must be restricted such as:

$$1 \leqslant 2\frac{1-v}{v} \tag{58}$$

giving the CFL condition

$$v \leqslant \frac{2}{3}. \tag{59}$$

The upper bound value of the limited Ψ function is then:

$$\Psi^{\mathrm{TVD}} = \max\left(0, \min\left(2\ r_{j+1/2}\frac{1-v}{v}, \Psi, 2\right)\right). \tag{60}$$

Let us remark that this condition is more restrictive than the one-step condition (16) for all values of v. One can either use this formula, or fix the coefficient $\alpha = (1-v)/v$ to its minimum value. For example, for CFL values lower than 0.5, we have $\alpha_{\min} = 1$ and one can take $\Psi^{\mathrm{TVD}} = \max(0, \min(2\ r_{j+1/2}, \Psi, 2))$ which allows all the classical (second-order accurate) limiters to be used to express Ψ^{TVD}.

In the followings, we will denote by $\Psi^{\mathrm{TVD}}_{\alpha}$ the function

$$\Psi^{\mathrm{TVD}}_{\alpha} = \max(0, \min(2\ \alpha\ r_{j+1/2}, \Psi, 2)). \tag{61}$$

In order to obtain a TVD scheme at each step of the Runge–Kutta solver, v must then be restricted such that $v \leqslant 1/(1+\alpha)$.

These TVD conditions, identical to the non-relaxed geometrical conditions in [25], correspond to

$$\gamma^+ = \frac{1}{2}\Psi_{j+1/2} \quad \text{and} \quad \gamma^- = \frac{1}{2}\Psi_{j+1/2}\frac{1}{r_{j+1/2}}\frac{v}{1-v}$$

in (18) and (21).

This shows that the MP conditions derived in [25] can be expressed as constraints acting on the Ψ function. The procedure is similar to the one followed in the one-step scheme by replacing the function Φ by Ψ, and must be performed for each stage of the Runge–Kutta scheme.

3. Extension of the one-step scheme to the Euler and Navier–Stokes equations

3.1. One dimension

The Euler system for 1D gas dynamics is written:

$$\frac{\partial w}{\partial t}+\frac{\partial f(w)}{\partial x}=0, \tag{62}$$

where $w=(\rho,\rho u,\rho E)^{\mathrm{T}}$ is the vector of conservative variables, ρ being the density, u the velocity, E the total energy linked to the pressure p by the perfect gas equation of state $p=(\gamma-1)\rho(E-\frac{1}{2}u^2)$ (the specific heat ratio γ is constant and equal to 1.4). The flux $f(w)$ is the vector $(\rho u,\rho u^2+p,(\rho E+p)u)^{\mathrm{T}}$.

In the following, we present the extension of the high order coupled time–space approach to the system of equations, by using the Roe flux difference splitting. We then describe the extension of the related TVD and MP constraints.

3.1.1. OSo scheme

The one-step scheme reads:

$$w_j^{n+1}=w_j^n-\frac{\delta t}{\delta x}(F_{j+1/2}-F_{j-1/2}), \tag{63}$$

where w_j^n is the local value of w in cell j at time $t=n\delta t$ and $F_{j+1/2}$ is the numerical flux of the scheme which is given by:

$$F_{j+1/2}=F_{j+1/2}^{\mathrm{Roe}}+\frac{1}{2}\sum_{k=1}^{3}(\Phi_k^o(1-\mid v_k\mid)\delta\mid f_k\mid \mathbf{r}_k)_{j+1/2} \tag{64}$$

with the first-order Roe flux defined as follows:

$$F_{j+1/2}^{\mathrm{Roe}}=\frac{1}{2}(f_j+f_{j+1})-\frac{1}{2}\sum_k(\delta\mid f_k\mid \mathbf{r}_k)_{j+1/2} \tag{65}$$

with

$$\delta|f_k|=|\lambda_k|\delta\alpha_k,$$

where δ is the forward difference operator ($\delta z_{i+1/2}=z_{i+1}-z_i$), λ_k and $\mathbf{r}_k$ are the eigenvalues and right eigenvectors of the Roe-averaged jacobian matrix $A=\mathrm{d}f/\mathrm{d}w$, $\delta\alpha_k$ is the kth Riemann invariant and $v_k=(\delta t/\delta x)\lambda_k$. Let us mention that, for clarity, the superscript n has been omitted in the expression of the fluxes.

The most direct way to extend the high order one step scheme to the non-linear system case uses a classical direct extension of the formula (11) with respect to each kth wave of the system, where v is replaced by $\mid v_k\mid$ and $r_{j+1/2}$ is replaced by $r_{j+1/2,k}^s$ with $s=\mathrm{sign}(\lambda_k)$. The ratio of the wave strengths $r_{j+1/2,k}^s$ is then defined as:

$$r_{j+1/2,k}^s=\frac{\delta\alpha_{k,j-s+1/2}}{\delta\alpha_{k,j+1/2}}.$$

This is the simplest and cheapest way to extend the scheme, but the drawback is that the formal order of accuracy in space is now only two, as we work in the eigenvector basis of the considered interface, i.e., we locally linearize the equations. The order of accuracy in time is also no more than two in this way, as we do not take into account the complicated non-linear terms that arise in the derivation of the modified equation of the Lax–Wendroff scheme.

Another way to extend the scheme would be to use the Cauchy–Kowalewski procedure for substituting time derivatives by space derivatives in the derivation of the successive modified equations. This procedure, described in [9], should allow the extension of the scheme to the non-linear system case while keeping the same order of accuracy. However, the procedure is very complex, especially in the multidimensional case. Also, the TVD (and MP as a consequence) conditions are not directly extensible in 2D, except if a time splitting strategy is used. In view of these problems, we choose here to keep the level of complexity of the scheme comparable to classical second-order TVD schemes. This point could be the subject of further studies, but as we will show in the following we have obtained very good numerical results using this simple method of extension.

3.1.2. OSTVDo scheme

The TVD constraints are written for each characteristic field as in the non-linear scalar case

$$\Phi^{o\text{-TVD}}_{j+1/2,k} = \max\left(0, \min\left(\frac{2r^s_{j+1/2,k}}{\mid v_{j+1/2,k}\mid}\frac{1-\mid v_{j-s+1/2,k}\mid}{1-\mid v_{j+1/2,k}\mid}, \Phi^o_{j+1/2,k}, \frac{2}{1-\mid v_{j+1/2,k}\mid}\right)\right). \tag{66}$$

3.1.3. OSMPo scheme

The monotonicity constraints are extended by rather working on the flux difference components:

$$\delta F_{j+1/2,k} = F_{j+1/2,k} - F^{\text{Roe}}_{j+1/2,k} = \frac{1}{2}\Phi^o_{j+1/2,k}(1-\mid v_{j+1/2,k}\mid)\delta\mid f_{j+1/2,k}\mid. \tag{67}$$

We also express the values defining the monotonicity intervals as flux differences, following the work previously performed on the scalar case:

$$\delta f^{\text{ul}}_{j+1/2,k} = \frac{r^s_{j+1/2,k}}{\mid v_{j+1/2,k}\mid}(1-\mid v_{j-s+1/2,k}\mid)\delta\mid f_{j+1/2,k}\mid, \tag{68}$$

$$\delta f^{\text{md}}_{j+1/2,k} = \frac{1}{2}\delta\mid f_{j+1/2,k}\mid - \frac{1}{2}d_{j+1/2,k}, \tag{69}$$

$$\delta f^{\text{lc}}_{j+1/2,k} = \frac{1}{2}\delta f^{\text{ul}}_{j+1/2,k} + \frac{1}{2}\frac{1-\mid v_{j-s+1/2,k}\mid}{\mid v_{j+1/2,k}\mid}d_{j-s+1/2,k}, \tag{70}$$

where $d_{j+1/2,k}$ is given by (40) with however:

$$d_{j,k} = \lambda_{j+1/2,k}\delta\alpha_{j+1/2,k} - \lambda_{j-1/2,k}\delta\alpha_{j-1/2,k}. \tag{71}$$

Finally the values $\Phi^{\text{md}}_{j+1/2,k}$ and $\Phi^{\text{lc}}_{j+1/2,k}$ are given by:

$$\Phi^{\text{md}}_{j+1/2,k} = \frac{2}{1-\mid v_{j+1/2,k}\mid}\frac{\delta f^{\text{md}}_{j+1/2,k}}{\delta\mid f_{j+1/2,k}\mid}$$

and

$$\Phi^{\text{lc}}_{j+1/2,k} = \frac{2r^s_{j+1/2,k}}{\mid v_{j+1/2,k}\mid}\frac{1-\mid v_{j-s+1/2,k}\mid}{1-\mid v_{j+1/2,k}\mid}\frac{\delta f^{\text{lc}}_{j+1/2,k}}{\delta f^{\text{ul}}_{j+1/2,k}}.$$

This completes the extension to systems.

3.2. Two dimensions

The treatment of the multidimensional case is straightforward in the case of separate time–space discretization, if treated dimension by dimension (see [25]). However, the MP conditions rely on TVD conditions as we have shown in the preceding section. TVD conditions are not directly extensible in the multidimensional case, and Locally Extremum Diminishing conditions should rather be considered, but this would lead to additional stability restrictions. This implies that the direct extension of the MP conditions does not guarantee that the resulting scheme will be non-oscillatory.

Following the one-step approach, the multidimensional extension is even more delicate, since we have to consider cross derivative terms that appear in the second and higher order terms, which are left uncontrolled if one applies a direction by direction TVD correction to a Lax–Wendroff unsplit scheme. A Locally Extremum Diminishing scheme can be obtained if one discretizes the mixed terms using upwind formulae, but it is very difficult to implement and our preliminary numerical experiments in this way did not give good results. The simplest way to avoid the problem of cross derivatives and to recover the good properties of the 1D scheme is to use a Strang directional splitting strategy, which is only second-order accurate. In two dimensions, the Euler system is written:

$$\frac{\partial w}{\partial t}+\frac{\partial f(w)}{\partial x}+\frac{\partial g(w)}{\partial y}=0, \tag{72}$$

where f and g are the fluxes in each direction. We implement the splitting as follows:

$$w_j^{n+2}=L_{\delta x}L_{\delta y}L_{\delta y}L_{\delta x}w_j^n, \tag{73}$$

where $L_{\delta x}$ (resp. $L_{\delta y}$) being a discrete approximation of $L_x(w)=-f(w)_x$ (resp. $L_y(w)=-g(w)_y$). In such a way, the second-order accuracy is recovered every two time steps.

4. Numerical results

4.1. The 1D scalar case

4.1.1. A convergence study for a smooth initial profile

We solve the advection Eq. (1) on the domain $[-1,1]$ with initial condition $u_0(x)=\sin^4(\pi x)$ and periodic boundary conditions. The computed L_1 error and order of accuracy are listed in Table 1 (the CFL number is equal to 0.5). The results for the OSTVD7 scheme show that the TVD constraints lower the order of accuracy to around 2.5. We note that the OSMP7 scheme equipped with $d_{j+1/2}=d_{j+1/2}^{\mathrm{MM}}$ gives the same results as the OS7 scheme, and that both schemes reach the theoretical seventh order of accuracy. The use of $d_{j+1/2}=d_{j+1/2}^{\mathrm{M4}}$ has the effect of lowering the order for the finest meshes. Compared to the results given in [2] for this test case, the OSMP7 scheme has errors at least one order of magnitude lower than the MPWENO5 scheme.

4.1.2. Advection of an initial profile with discontinuities

We now consider the classical test case of the advection of an initial profile composed of a Gaussian wave, a square wave, a triangular wave and an ellipse. This is a difficult test case because it includes discontinuities as well as smooth portions of curves and extrema. The initial condition $u_0(x)$ is defined on the interval $x\in[-1,1]$ as:

Table 1
Advection of the initial condition $u_0(x) = \sin^4(\pi x)$: L_1 error and order of accuracy for the one-step schemes

Method	Number of grid points	L_1 error	L_1 order
OS7	20	5.16494×10^{-3}	
OSMP7	40	5.66989×10^{-5}	6.51
$d_{j+1/2} = d^{\mathrm{MM}}_{j+1/2}$	80	4.74407×10^{-7}	6.90
	160	3.76700×10^{-9}	6.98
	320	2.95501×10^{-11}	6.99
OSMP7	20	5.08530×10^{-3}	
$d_{j+1/2} = d^{\mathrm{M4}}_{j+1/2}$	40	5.67752×10^{-5}	6.48
	80	6.84954×10^{-7}	6.37
	160	2.19588×10^{-8}	4.96
	320	1.33241×10^{-9}	4.04
OSTVD7	20	2.13730×10^{-2}	
	40	3.85456×10^{-3}	2.47
	80	7.78303×10^{-4}	2.31
	160	1.47891×10^{-4}	2.40
	320	2.73871×10^{-5}	2.43

$$\begin{cases} u_0(x) = \exp(-\log(2)(x+0.7)^2/0.0009) & \text{if } -0.8 \leqslant x \leqslant -0.6, \\ u_0(x) = 1 & \text{if } -0.4 \leqslant x \leqslant -0.2, \\ u_0(x) = 1 - |10(x-0.1)| & \text{if } 0 \leqslant x \leqslant 0.2, \\ u_0(x) = (1 - 100(x-0.5)^2)^{1/2} & \text{if } 0.4 \leqslant x \leqslant 0.6, \\ u_0(x) = 0 & \text{otherwise} \end{cases} \tag{74}$$

and periodic boundary conditions are prescribed. We use a uniform grid composed of 200 mesh-cells. The solutions obtained at two dimensionless times $t = 20$ (10 periods) and $t = 100$ (50 periods) are shown in Figs. 1–5. Let us emphasize that this corresponds to long time integration, as usually only 10 periods are presented for this test case.

Among the schemes described above, we present the results obtained using three of them (and their TVD and monotonicity-preserving variants): the one-step seventh-order scheme (named OS7), and the multistage RK3 scheme associated with a fifth order (RK3/5) and a seventh order (RK3/7) in space discretization. We will denote by OSTVD7 and OSMP7, respectively, the TVD and monotonicity-preserving variants of the OS7 scheme. We will also denote by RK3/TVD5(α) (respectively RK3/TVD7(α)) the TVD versions of the multistage schemes, and by RK3/MP5(α) (respectively RK3/MP7(α)) their MP versions; here the notation (α) is relative to the coefficient of the limited function $\Psi^{\mathrm{TVD}}_{\alpha}$. For comparison, we have also performed a calculation using a RK3/WENO($r = 5$) [10] scheme.

Let us first compare the CPU times needed for each scheme to compute 20,000 time steps, it takes: 22.83 s using the OS7 scheme, 25.31 s for the OSTVD7 scheme, 33.77 s for the OSMP7 scheme, 39.37 s for the RK3/TVD5 scheme and 46.23 s for the RK3/TVD7 scheme. This means that it takes nearly twice the time to get a seventh order in space approximation using a multistage scheme compared to a one-step scheme (and a larger stencil is necessary).

Fig. 1 shows the results obtained for the three versions of the one step seventh-order scheme and the RK3/WENO5 scheme, using a CFL number equal to 0.1. The OS7 gives very good results, except for numerical oscillations in the discontinuous regions. The TVD correction does a very good job of eliminating these oscillations, but tends to smooth extrema, although this is very localized. The MP correction is almost perfect, keeping the properties of the TVD correction while leaving unchanged the extrema compared to the original scheme. The discontinuities are represented over six points, which is rather low

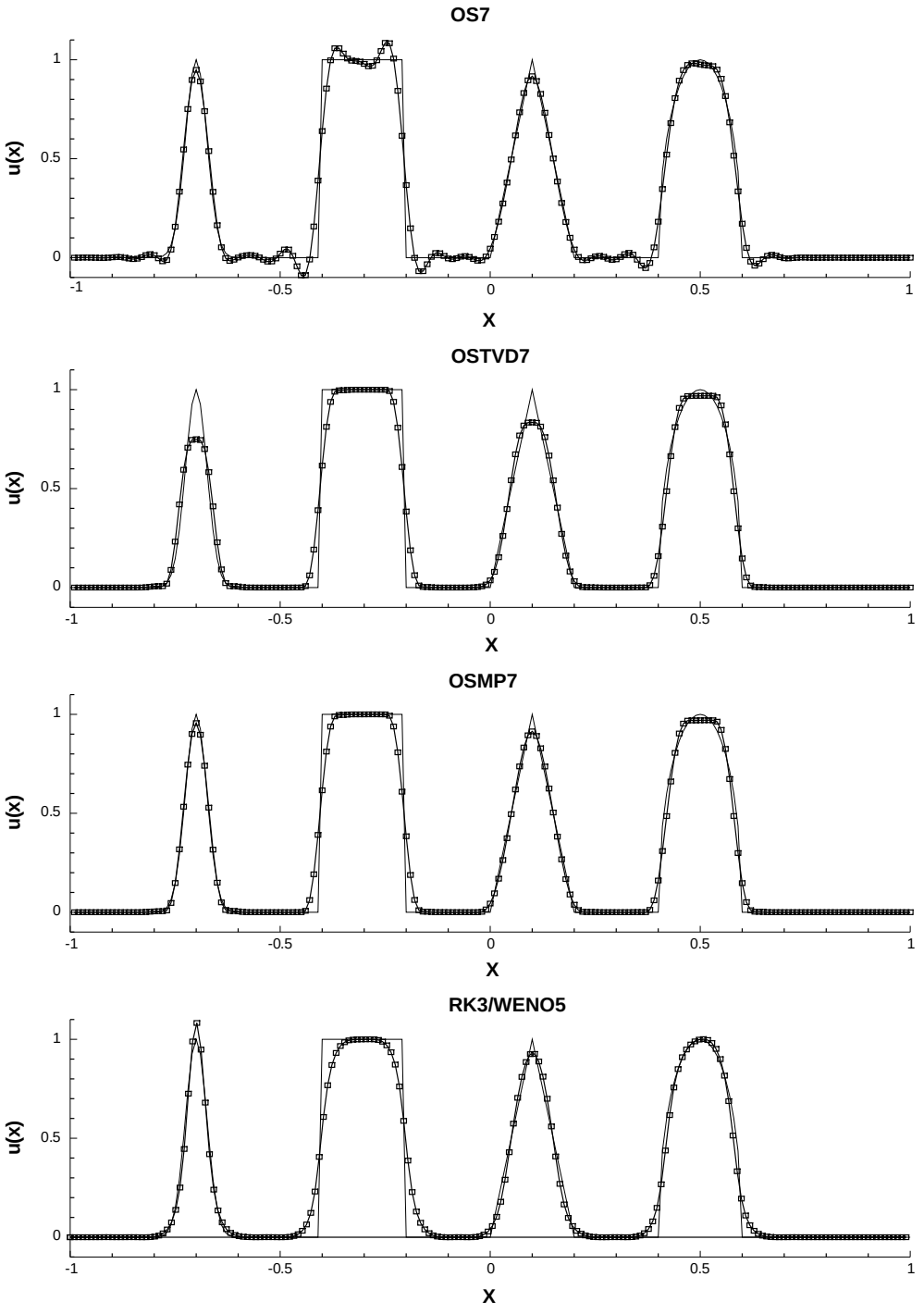

Fig. 1. Advection over 10 periods ($t = 20$). From top to bottom: Seventh-order one-step scheme (OS7), the corresponding TVD (OSTVD7) and MP (OSMP7) schemes, a RK3/WENO5 scheme. All the schemes are used with CFL = 0.1.

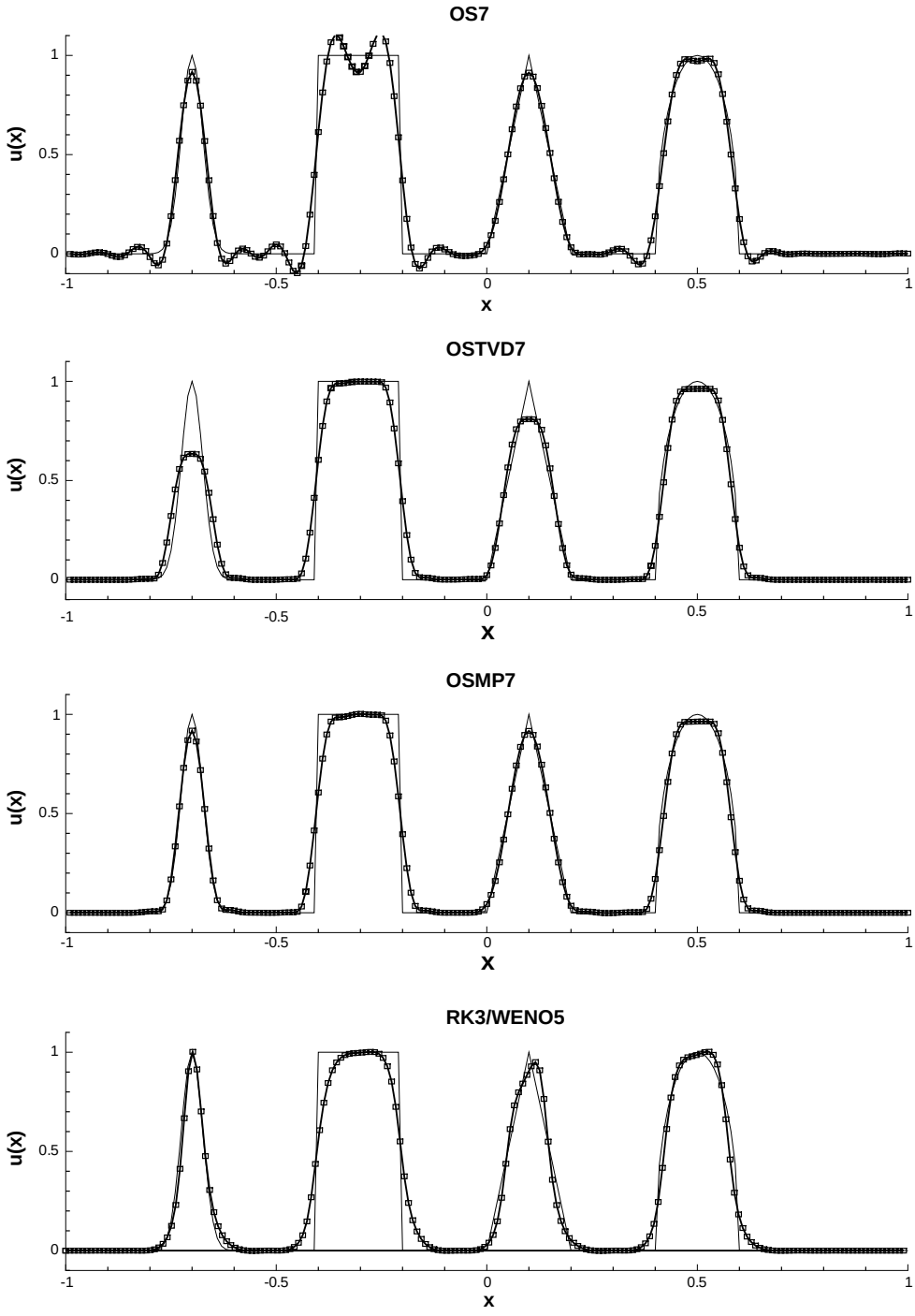

Fig. 2. Advection over 50 periods ($t = 100$). From top to bottom: Seventh-order one-step scheme (OS7), the corresponding TVD (OSTVD7) and MP (OSMP7) schemes, a RK3/WENO5 scheme. All the schemes are used with CFL = 0.1.

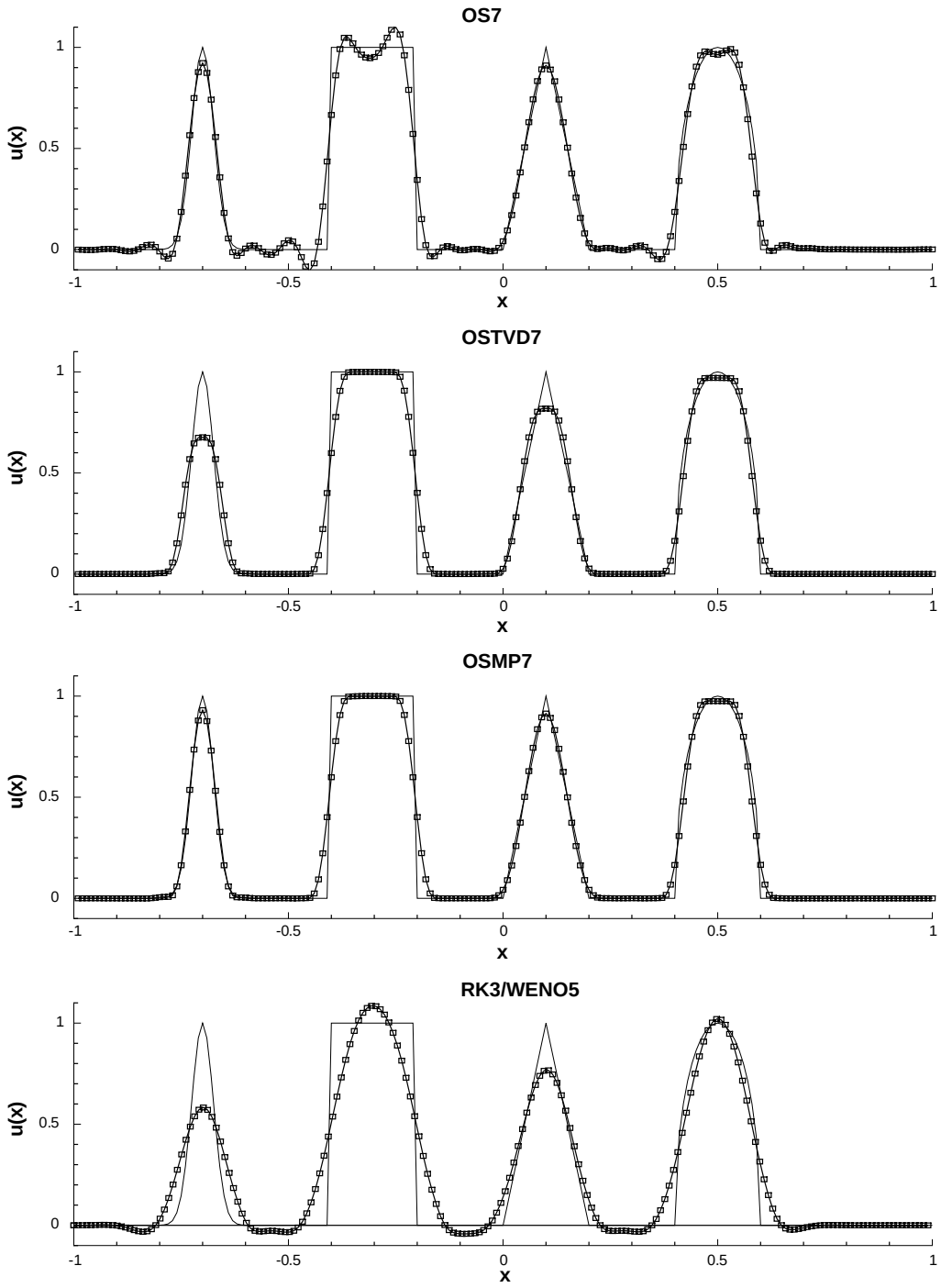

Fig. 3. Advection over 50 periods ($t = 100$). From top to bottom: Seventh-order one-step scheme (OS7), the corresponding TVD (OSTVD7) and MP (OSMP7) schemes, a RK3/WENO5 scheme. All the schemes are used with CFL = 0.5.

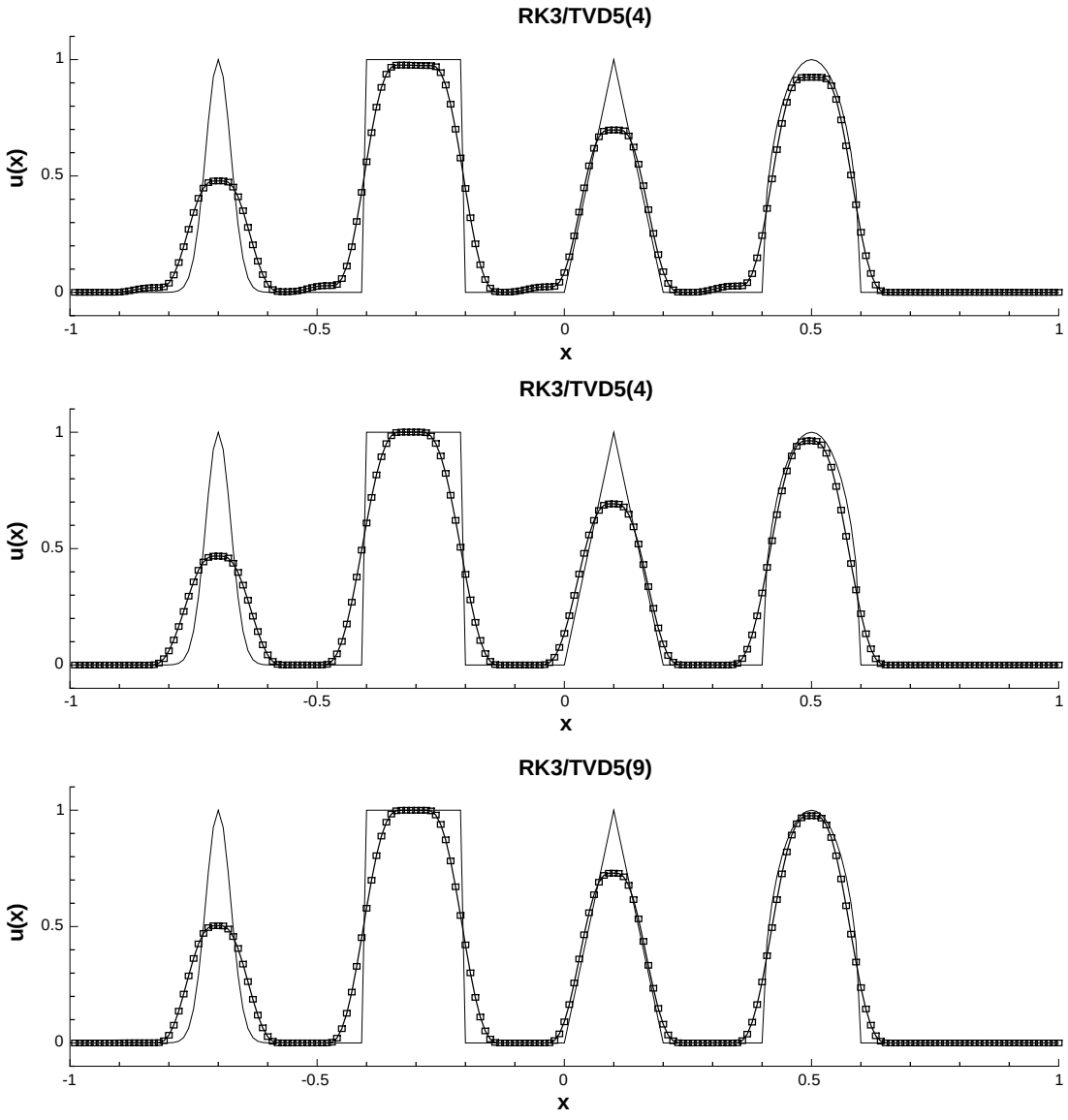

Fig. 4. Advection over 50 periods ($t = 100$). Fifth-order TVD multistage scheme: RK3/TVD5(4) with CFL = 0.1 (top) and CFL = 0.4 (middle), RK3/TVD5(9) with CFL = 0.1 (bottom).

after 20,000 time iterations. The same conclusions can be made after 50 periods (Fig. 2). The discontinuities are a little more smeared (eight points), and one can notice a small staircasing effect around the corners which is due to diffusive effects at low CFL numbers. But the solution can still be considered of excellent quality. The quality of the results given by the OSMP7 scheme is even better at higher CFL number as shown in Fig. 3 for CFL = 0.5. If we now compare these results with those given by the RK3/WENO5 scheme, it is apparent that, while the WENO scheme is very successful in representing extrema (sometimes without control as can be seen in Fig. 1), it is more diffusive around discontinuities and tends

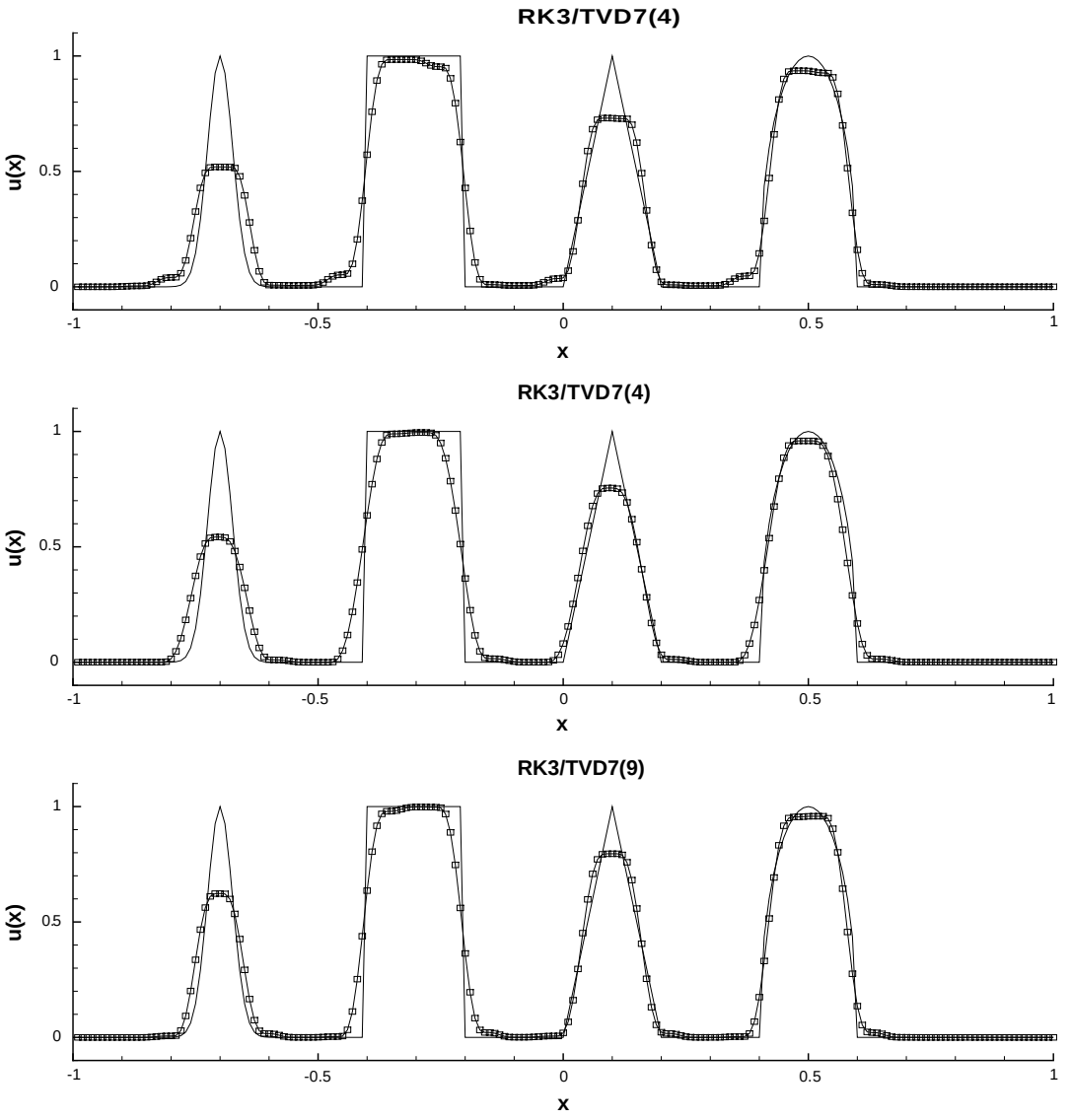

Fig. 5. Advection over 50 periods ($t = 100$). Seventh-order TVD multistage scheme: RK3/TVD7(4) with CFL = 0.1 (top) and CFL = 0.4 (middle), RK3/TVD7(9) with CFL = 0.1 (bottom).

to round the corners. One can also remark that the error of this scheme increases with the CFL number (Fig. 3), unlike the OS7 scheme.

Let us now compare these results with those obtained using the RK3/TVD and MP schemes. Figs. 4 and 5 show the numerical solution after 50 periods given by the RK3/TVD5 and TVD7 schemes, using the two values $\alpha = 4$ and $\alpha = 9$. For the case $\alpha = 4$, the scheme will be TVD provided that $\nu \leqslant 0.2$. In fact, as can be seen on the results, this CFL constraint is too restrictive, as it does not take into account the dissipation added by the temporal scheme. The results are better using CFL = 0.4 than CFL = 0.1, which means that the errors of the spatial and temporal scheme compensate for CFL = 0.4, while the total dissipative error is

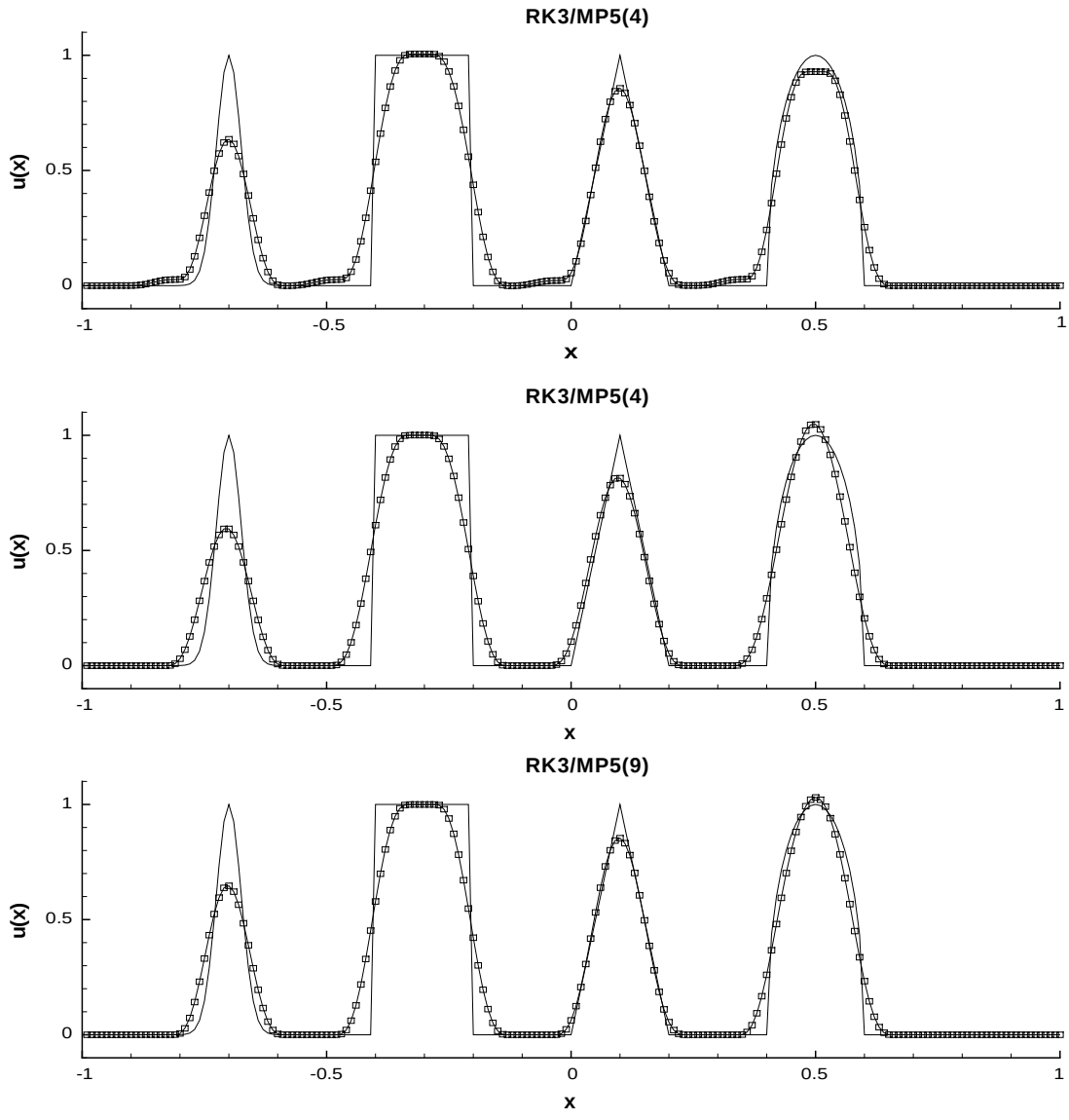

Fig. 6. Advection over 50 periods ($t = 100$). Fifth-order MP multistage scheme: RK3/MP5(4) with CFL = 0.1 (top) and CFL = 0.4 (middle), RK3/MP5(9) with CFL = 0.1 (bottom).

too large if the scheme is step by step TVD. More precisely, in the multistage approach the dissipation added by the temporal scheme is not included in the derivation of the TVD or MP constraints. As a consequence, the TVD/MP corrections will be switched on more often that would really be necessary, contrary to what happens in the one-step approach. This phenomenon is accentuated when the spatial order of the scheme is increased, as can be seen by comparing the fifth- and seventh-order results, showing that the staircasing due to the dissipative error is greater in the seventh-order case. Let us also remark that it is interesting to increase the value of α to improve the results (see the results using $\alpha = 9$), but this implies a lowering of the CFL number (the scheme is TVD at each time step if $v \leqslant 0.1$ for $\alpha = 9$). Finally, Fig. 6 shows the results obtained by using the RK3/MP5 scheme. While these results are much better than the

corresponding TVD results shown in Fig. 4, the same remark can be made for the role of the dissipative temporal error.

In conclusion, among the schemes we compared, the one-step scheme gives the best results, at the lowest cost. The control of the total truncation error allowed by the one step approach leads to the derivation of optimal non-oscillatory conditions.

4.2. 1D Euler equations

4.2.1. Shock wave interacting with a density disturbance

In this test case, which was proposed in [21], a moving Mach 3 shock wave interacts with a sinusoidal density profile. It is a difficult test case because it involves both a shock and smooth structures. The 1D Euler equations are solved on the spatial domain $x \in [0, 10]$. The solution is initially prescribed as

$$\begin{cases} \rho = 3.857, & u = 2.629, \quad p = 10.3333 & \text{when } x < 1, \\ \rho = 1 + 0.2\sin(5x), & u = 0, \quad p = 1 & \text{when } x \geqslant 1. \end{cases}$$

The computation is stopped at a dimensional time $t = 1.8$. Fig. 7 presents the results obtained by using the three versions of the OS7 scheme (OS7, OSTVD7, OSMP7) and the RK3/WENO5 scheme [10], for 200

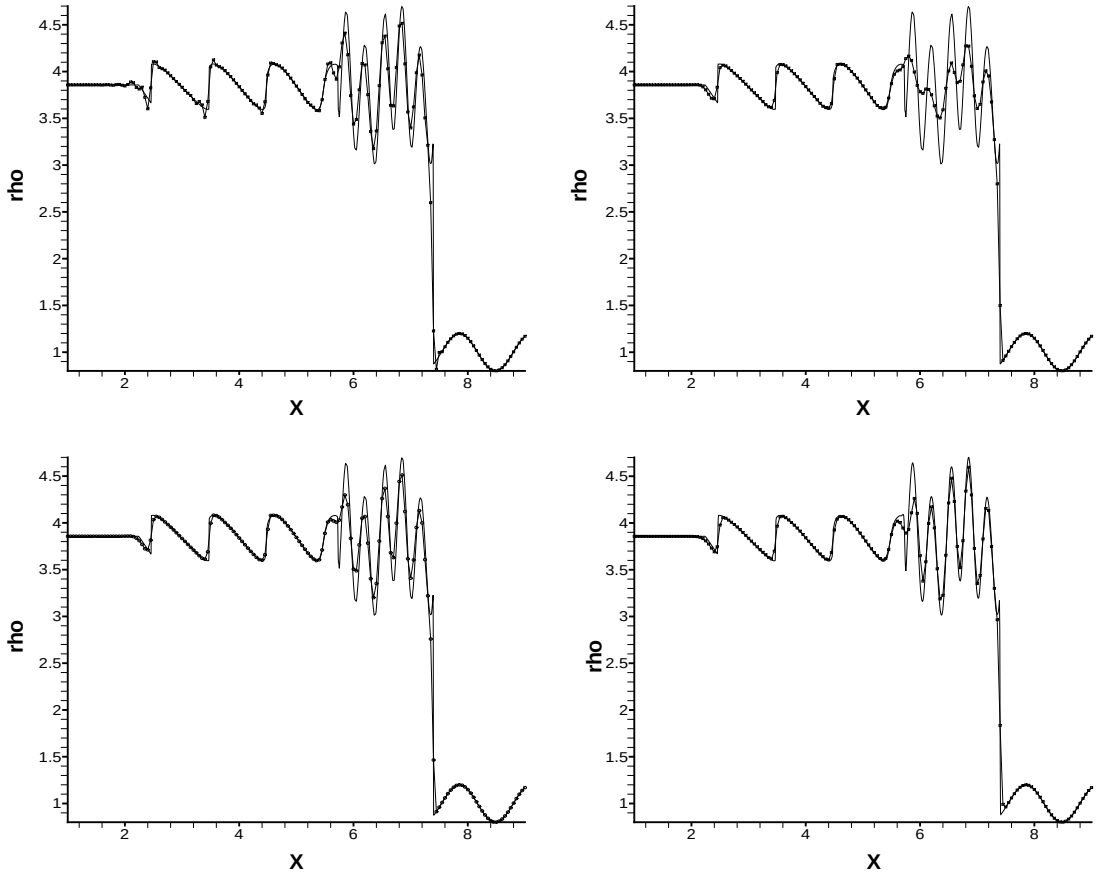

Fig. 7. Density distribution for the first Shu–Osher test case at $t = 1.8$, 200 grid points, CFL = 0.5. Top left: OS7 scheme, top right: OSTVD7 scheme, bottom left: OSMP7 scheme, bottom right: RK3/WENO5 scheme.

grid cells. This is a very coarse grid in which classical TVD schemes retain almost none of the structures immediately behind the shock wave. We can see here that the OSMP7 does a very good job, by eliminating the spurious oscillations generated by the OS7 base scheme, while relaxing the TVD constraints where they are not useful and "clip" the extrema. The OSMP7 results here are very close to those given by the RK3/WENO5 scheme, which is very good for this test case.

In Fig. 8 are compared the results for the OSMP7 and RK3/WENO5 schemes using 400 grid cells. One can conclude that both schemes have practically converged on this mesh, but at a lower cost for the OSMP7 scheme which is about five–six times less expensive than the RK3/WENO5 scheme. To be more precise, we have counted the number N of floating point operations needed per grid point and per time iteration in each case. The results are the following: the value of N is 1641 for RK3/WENO3, 3725 for RK3/WENO5, 541 for OSTVD7, 670 for OSMP7 and 354 for a one-step Van Leer second-order flux limiter scheme. Each stage of the RK3/WENO5 scheme costs roughly twice a time iteration of the OSTVD7 scheme. The added cost for the MP algorithm can be approximated by the difference $N(\text{OSMP7}) - N(\text{OSTVD7})$, so we can estimate a N-value close to 4100 for the RK3/MPWENO5 scheme, six times that of the OSMP7 scheme.

Let us also present the results we obtained for a variant of this test case that is often considered in place of the first one. The spatial domain is now the interval $[-1, 1]$ and the initial state is

$$\begin{cases} \rho = 3.857, & u = 2.629, \quad p = 10.3333 & \text{when } x < -0.8, \\ \rho = 1 + 0.2\sin(5\pi x), & u = 0, \quad p = 1 & \text{when } x \geqslant -0.8. \end{cases}$$

The computation is stopped at a dimensional time $t = 0.47$. A grid with 200 zones is used. This test case is for example treated using a RK3/MPWENO5 scheme in [2]. We can compare this result in [2] (Fig. 4(a)) to the OSMP7 result shown in Fig. 9, and conclude that they are quite similar. We also have shown in Fig. 9 the result given by a classical second-order TVD scheme equipped with a Van Leer limiter, in order to highlight the increase of accuracy due to the OSMP7 scheme.

4.2.2. Lax shock tube

The previous test case is not very demanding of the robustness of the scheme, as the shock wave is rather weak. This is not the case for Lax's problem, which we have treated to highlight this point. The spatial domain is $[0, 2]$ and the initial conditions are defined as:

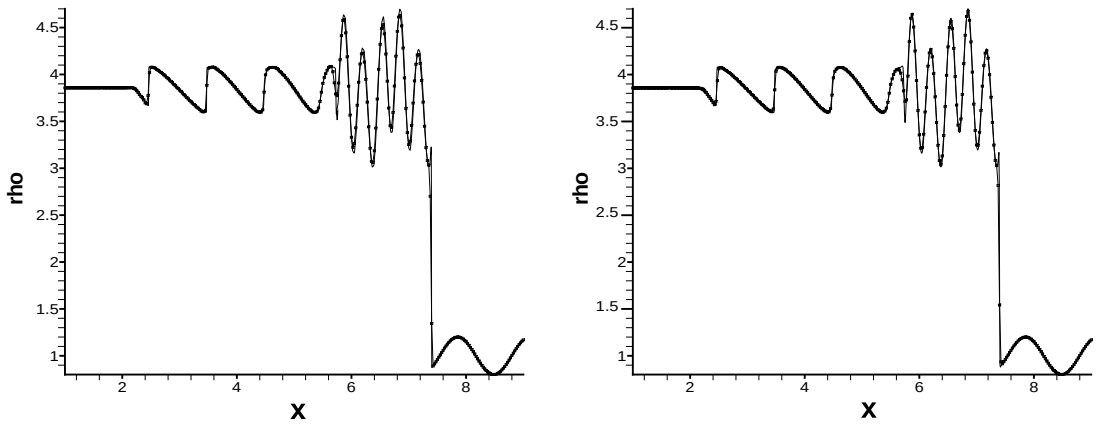

Fig. 8. Density distribution for the first Shu–Osher test case at $t = 1.8$, 400 grid points, CFL = 0.5. Left: OSMP7 scheme, right: RK3/WENO5 scheme.

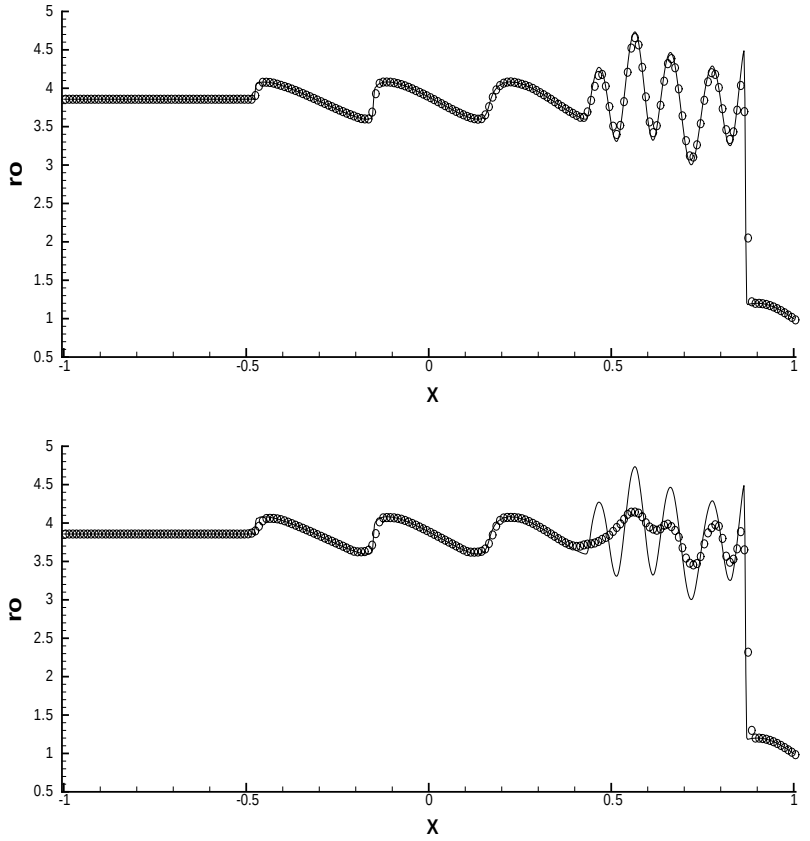

Fig. 9. Density distribution for the second Shu–Osher test case at $t = 0.47$, 200 grid points, CFL = 0.5. Top: OSMP7 scheme, bottom: TVD/Van Leer second-order scheme.

$$\begin{cases} \rho = 0.445, & u = 0.698, & p = 3.528 & \text{when } x < 1, \\ \rho = 0.5, & u = 0, & p = 0.571 & \text{when } x \geqslant 1. \end{cases}$$

The results are shown in Fig. 10 at time 0.32, for the OSMP7 scheme and three RK3/WENO3/5/7 schemes. One can observe that the best results are given by the OSMP7 scheme, the WENO results being more diffusive around the discontinuities or oscillatory for the WENO7. The MP strategy should give good results here applied to the WENO scheme as was done in [2], but with a higher computational effort.

4.3. 2D Euler and Navier–Stokes equations

4.3.1. Convergence study for a 2D Euler case

We consider the test case, treated in [2], of the propagation at 45° to the grid lines of a strong vortex at a supersonic Mach number. The vortex is initially centered in a domain $[-5,5] \times [-5,5]$. It is defined as a fluctuation to an unperturbed flow with $(\rho, p, u, v) = (1, 1, 1, 1)$, given by

$$(\delta u, \delta v) = \frac{\epsilon}{2\pi} e^{0.5(1-r^2)}(-y, x), \quad \delta T = -\frac{(\gamma-1)\epsilon^2}{8\gamma\pi^2} e^{(1-r^2)}, \quad \delta S = 0,$$

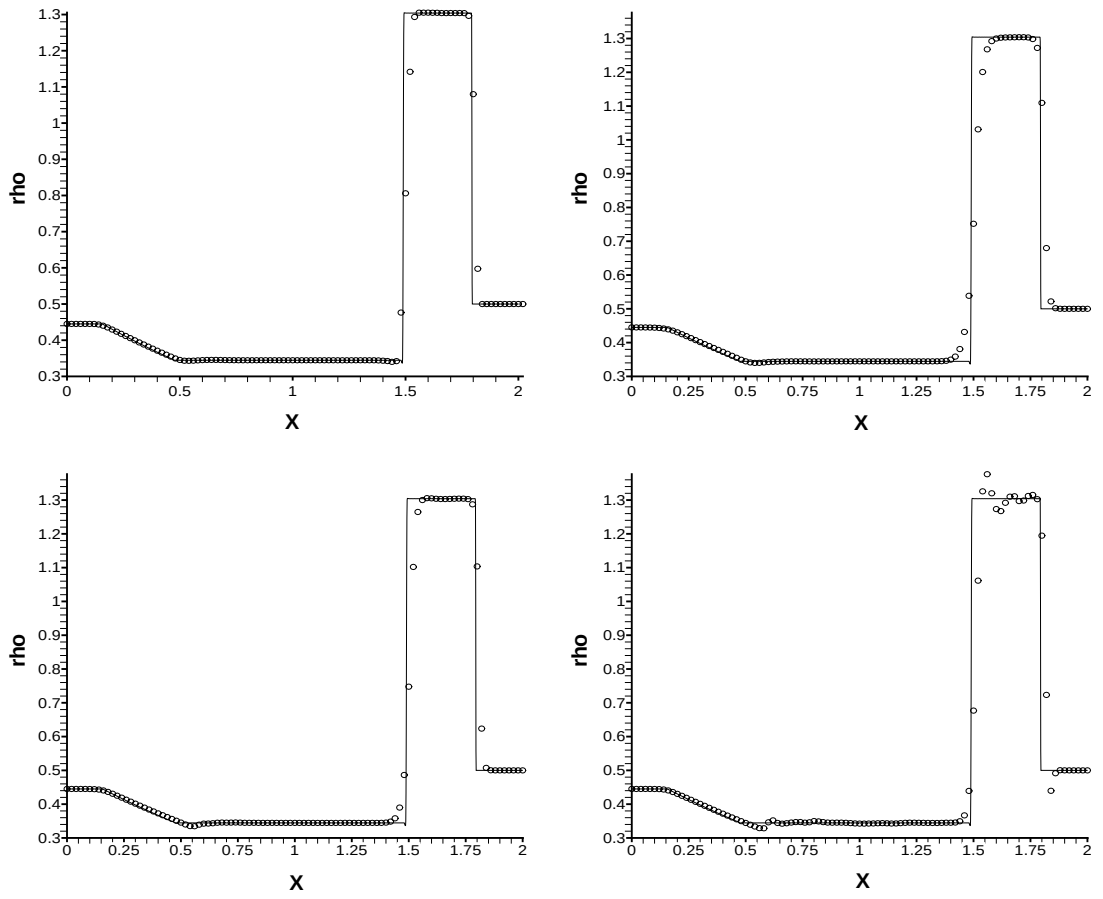

Fig. 10. Density distribution for the Lax test case at $t = 0.32$, 100 grid points, CFL = 0.5. Top, left: OSMP7 scheme, right: RK3/WENO3 scheme. Bottom, left: RK3/WENO5 scheme, right: RK3/WENO7 scheme.

where $r^2 = x^2 + y^2$, $S = p/\rho^\gamma$ is the entropy and $T = p/\rho$ is the temperature, $\gamma = 1.4$, $\epsilon = 5$ is the vortex strength. Periodic boundary conditions are imposed. The exact solution of this problem is just the passive convection of the vortex. The errors are calculated at time $t = 10$.

In Table 2 are listed the L_1 and L_∞ errors, together with the L_1 order of accuracy, obtained using the OSMP7 with $d_{j+1/2} = d^{M4}_{j+1/2}$. One can see that the scheme is only second-order accurate, due to the simplified extension to the non-linear system case. Nevertheless, as we have seen in the 1D Euler case, the quantitative values of the error are indeed much lower than for a classical second-order scheme. In Fig. 11 are represented the convergence curves associated with several schemes. The values for the WENO schemes are taken from [2]. One can see that, although the WENO schemes keep a high order of accuracy even in the 2D non-linear system case, their level of error is higher when the mesh is coarse. This implies that the OSMP7 scheme is more accurate than the WENO3 scheme for all the considered meshes. The MPWENO5 scheme has a lower error than the OSMP7 scheme for meshes finer than about 60×60. Considering also the lower cost of the OSMP7 scheme, this shows that it can be profitable to use the OSMP7 scheme, in cases where it is not possible to use very fine meshes (which is a very standard case, for example in LES calculations where all the length scales are not fully resolved). Using the argument developed in [2] that the flow features should be simulated with at least 1% accuracy for the purpose of LES calculations, we can see

Table 2
Transport of a strong vortex in supersonic flow: L_1 error and order of accuracy, L_∞ error for the OSMP7 scheme

Method	Number of grid points	L_1 error	L_1 order	L_∞ error
OSMP7	25×25	1.37×10^{-3}		1.67×10^{-2}
$d_{j+1/2} = d^{M4}_{j+1/2}$	50×50	3.13×10^{-4}	2.13	3.55×10^{-3}
	75×75	1.38×10^{-4}	2.02	1.66×10^{-3}
	100×100	7.73×10^{-5}	2.01	9.11×10^{-4}

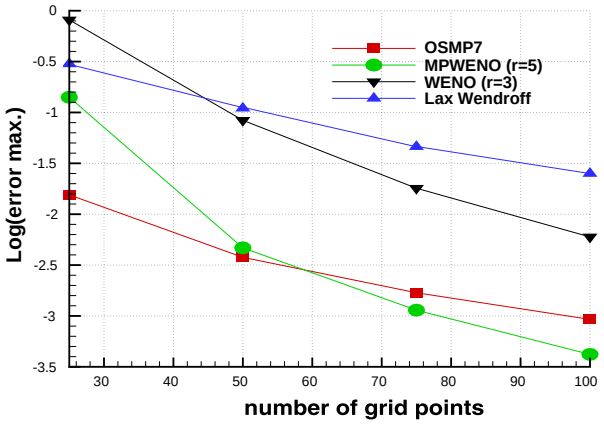

Fig. 11. Convergence curves for several schemes.

that the OSMP7 scheme achieves this level of error on the coarsest 25×25 grid (all flow variables are of the order of unity).

4.3.2. Double Mach reflection

This test case was solved using several numerical schemes for comparison in [28]. Solutions obtained using very fine meshes can also be found in [6]. The domain has a dimension $[0,4] \times [0,1]$. The problem involves a Mach 10 shock wave in air ($\gamma = 1.4$), which initially makes a 60° angle with the horizontal axis. The shock intersects the axis at $x = 1/6$. The region from $x = 0$ to $x = 1/6$ is always assigned the initial values. The region $x \in [1/6, 4]$ is a reflecting wall. The exact solution is set up and driven at the top of the domain. The computation stops at time 0.2. It is a difficult test case, involving both strong shocks and multiple stems. A jet forms along the wall, which is also very difficult to compute properly.

The results for this test case are shown in Fig. 12, where the density contours obtained using four grids with increasing resolution are represented. One can remark that all the features of the flow are captured at the correct position in the coarsest mesh. The shocks are very sharply captured, including the weak shock in the secondary Mach stem. There are some small oscillations in the nearly stationary zone underneath the curved shock wave, which is inherent to all schemes whose dissipation vanishes with zero flow velocity. If we compare our results with those in [25], for the 240×60 grid, we can conclude that they are very similar except that the wall jet is better represented in our calculation, if we refer to the results obtained using the finest grids.

As was pointed out in [2], this test case is difficult for schemes having Roe's scheme as the underlying first-order scheme. In fact, Roe's scheme systematically produces a carbuncle-type effect around the point

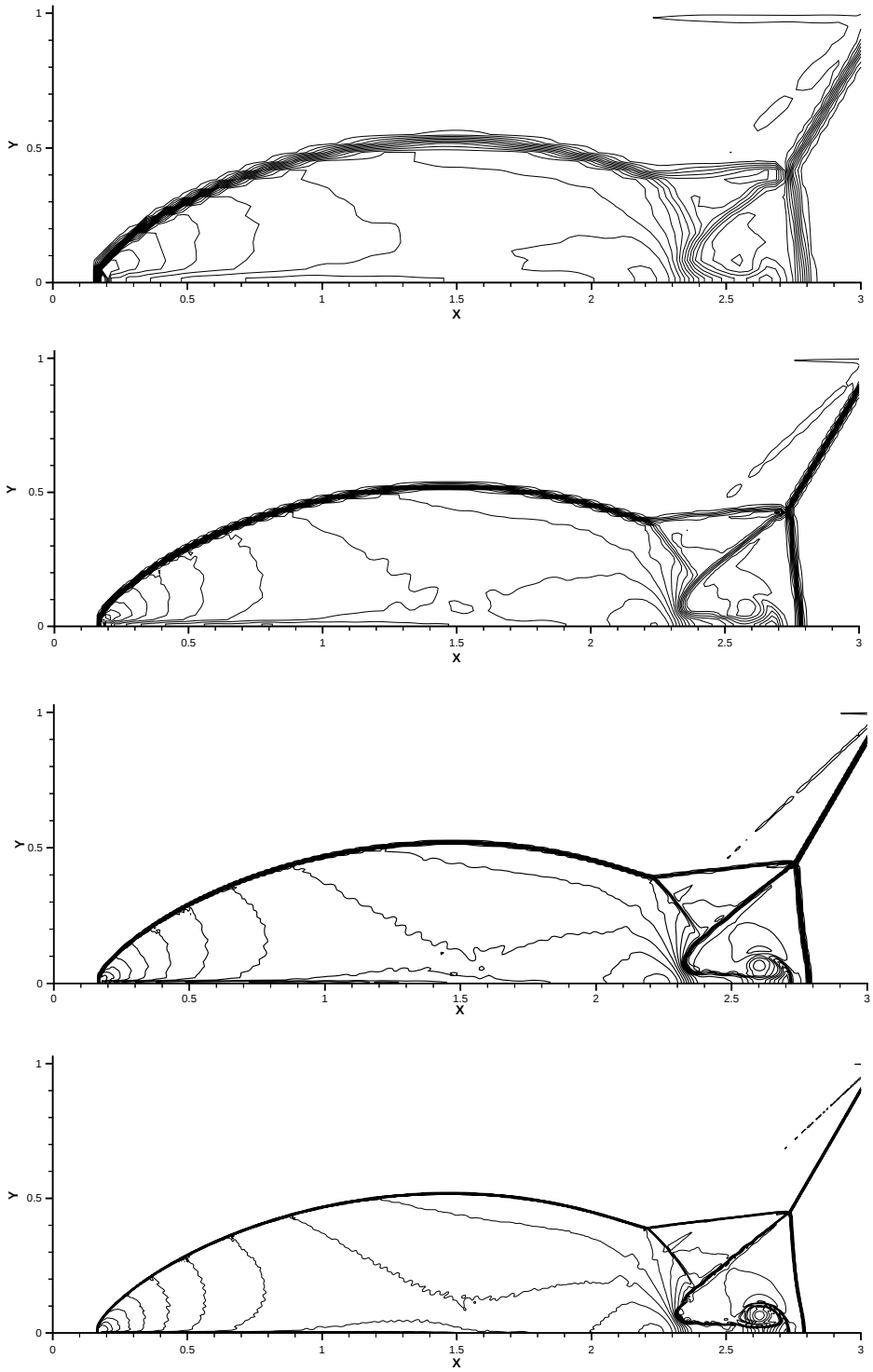

Fig. 12. Double Mach reflection, OSMP7 scheme. Density, 30 contours from 1.73 to 21, 120×30 grid, 240×60 grid, 480×120 grid, 960×240 grid from top to middle.

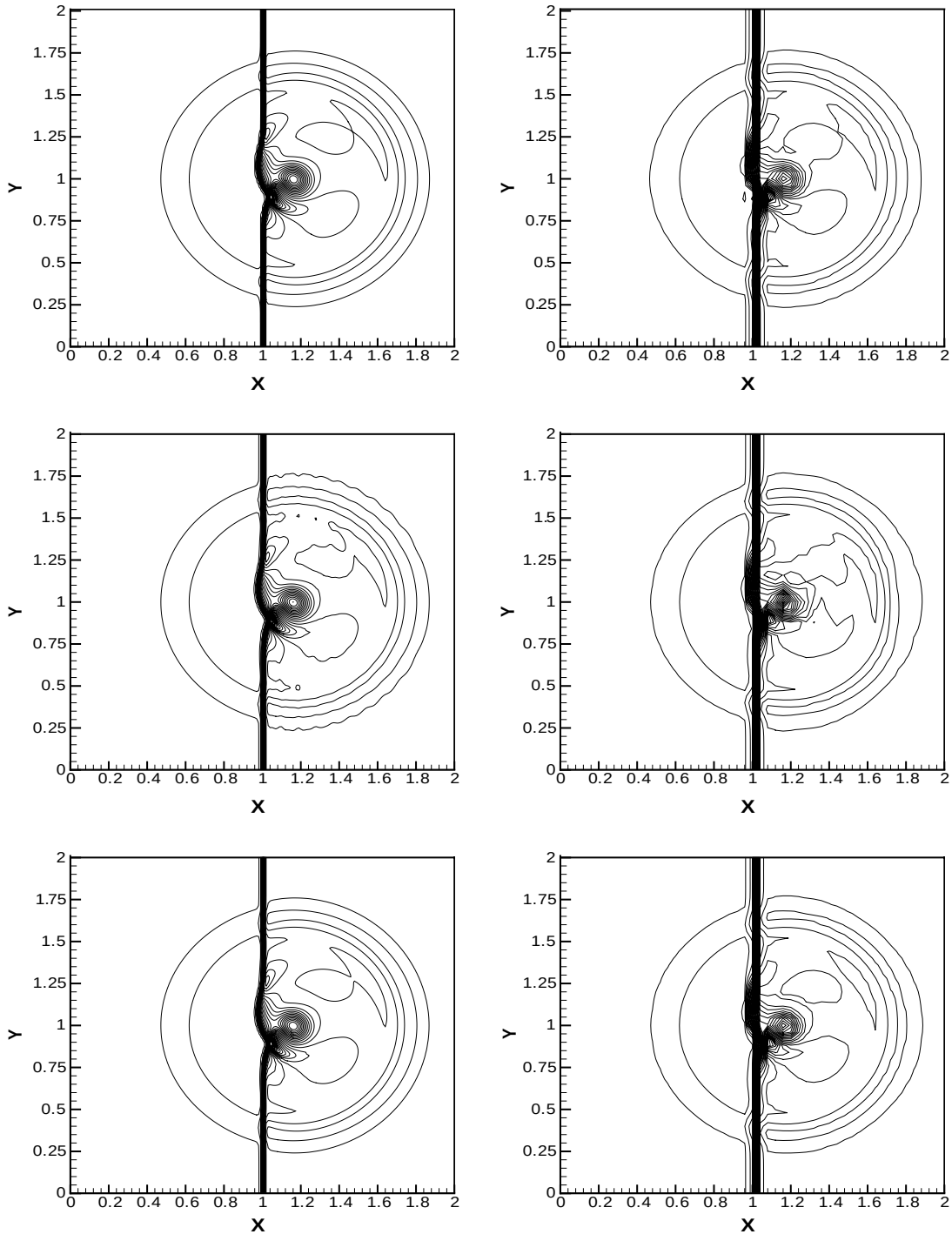

Fig. 13. Pressure contours for the 2D shock–vortex interaction at $t = 0.7$, CFL $= 0.5$ (49 contours from 0.527 to 0.845). Left: 200×200 grid points, right: 50×50 grid points. Top ,OSMP7 scheme; middle, RK3/WENO5 scheme; bottom, RK3/WENO7 scheme.

where the normal shock meets the wall. Curiously, this kind of problem was not encountered using the OSMP7 scheme in all the meshes we considered, whereas we could not obtain a correct solution using the WENO–Roe schemes in any grid (let us notice that we have added an entropy correction ([11]) to our OS scheme, which has a favorable effect on the problem). In [2] the Lax–Friedrichs (LF) scheme was used instead of Roe's scheme in order to avoid the problem (it is well known that the LF scheme is not prone to this phenomenon).

4.3.3. 2D viscous shock–vortex interaction

This test case, treated in [27], considers the viscous ($Re = 2000$) interaction of a plane weak shock with a single isentropic vortex. During the interaction, acoustic waves are produced, and we investigate the ability of the numerical scheme to predict and transport these waves. As this is a viscous flow, the Navier–Stokes equations are solved. In order to take the viscous terms easily into account, the one-step scheme is implemented as a Mac Cormack scheme followed by a correction, as was done in [7]. The viscous terms are discretized using centered second-order formulae.

The domain has a dimension $[0, 2L_0] \times [0, 2L_0]$, where L_0 is a reference length scale. The dimensionless computational domain is $[0, 2] \times [0, 2]$. A stationary plane shock is located at $x = 1$. The prescribed pressure jump through the shock is $\Delta P/P_\infty = 0.4$, where P_∞ is the static pressure at infinity, corresponding to a reference Mach number $M_0 = 1.1588$. The reference density and velocity are those of the free uniform flow at infinity. The Reynolds number, based on the reference length scale, density and velocity, is $Re = 2000$. An isolated Taylor vortex centered at $x_0 = \frac{1}{2}$, $y_0 = 1$ is initially superimposed on the base flow. The tangential velocity in the vortex is given by:

$$V_0(r) = C_1 r \cdot e^{-C_2 r^2} \tag{75}$$

with

$$C_1 = \frac{U_c}{r_c}, \quad C_2 = \frac{1}{2r_c^2}, \quad r = \sqrt{(x - x_0)^2 + (y - y_0)^2}.$$

The calculations were performed for $r_c = 0.075$ and $U_c = 0.25$. Periodic boundary conditions are applied in the y direction. The computations stopped at a dimensionless time $t = 0.7$.

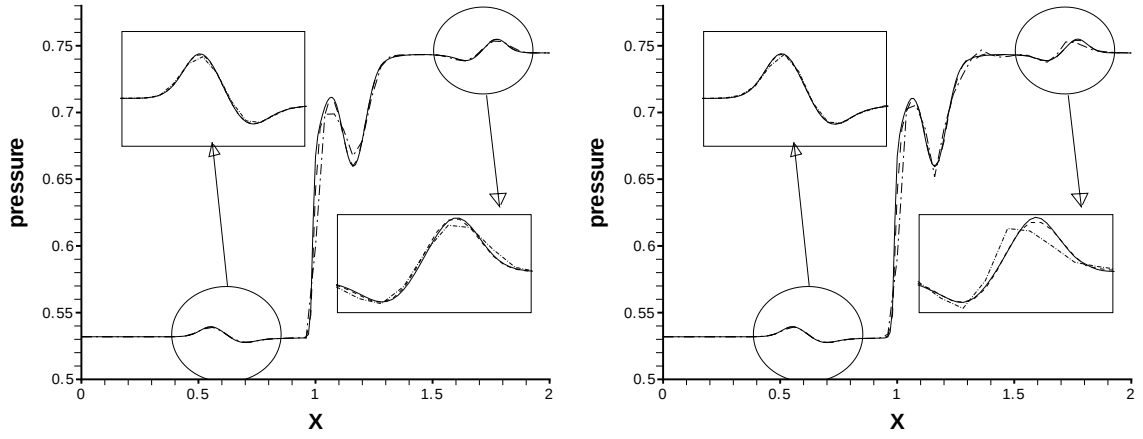

Fig. 14. Pressure along the line $y = 1$, 50×50 grid (dash-dotted line), 100×100 grid (dashed line), 200×200 grid (solid line); left: OSMP7 scheme, right: RK3/WENO5 scheme.

The pressure field contours obtained by using the OSMP7, RK3/WENO5 and RK3/WENO7 schemes are shown in Fig. 13, using 200×200 grid cells and 50×50 grid cells. One can notice the OSMP7 result is quite accurate even on a coarse grid and comparable to the WENO7 result. Curiously, the WENO5 scheme exhibits a slightly oscillatory behavior, which is not found in the WENO7 results. This can be seen more precisely on the pressure distribution along the line $y = 1$ (Fig. 14), which shows the high accuracy of the OSMP7 scheme in capturing the acoustic wave even on the coarsest grid. For this problem, the WENO5 scheme is seen to be insufficiently accurate on the coarse grid.

5. Conclusion

For the numerical simulation of unsteady compressible flows, we developed accurate numerical schemes based on a coupled time–space approach, which offer a compromise between high accuracy in smooth regions and an efficient shock capturing technique. We have shown that a coupled time and space approach for the solution of hyperbolic equations provides a very competitive numerical method compared to the state-of-the-art high resolution schemes (WENO, Runge–Kutta MP schemes). In the scalar case, a seventh-order accurate in time and space one-step scheme has been derived. When combined with MP conditions, the scheme has been shown to give very high quality results for long time integration. The MP conditions have then been extended from ([25]) to the case of a one-step scheme, and reinterpreted as TVD-like conditions in a flux limiting approach.

The extension of the one-step MP scheme to Euler and Navier–Stokes equations has been performed by using local linearization and dimensional splitting in the multidimensional case. Although this approach does not preserve the formal high order of accuracy of the scheme, it is shown to give very accurate results which compare well to high order WENO schemes, at a lower cost.

The investigated MP one-step schemes yield accurate results for the selected relevant test cases. However, one of the classical drawbacks associated with dimensional splitting is related to the treatment of boundary conditions for the intermediate step for bounded viscous flow calculations. This point is currently under investigation.

References

[1] M. Arora, P.L. Roe, A well behaved TVD limiter for high-resolution calculations of unsteady flows, Journal of Computational Physics 132 (1997) 2–11.
[2] D.S. Balsara, C.W. Shu, Monotonicity preserving weighted essentially non-oscillatory schemes with increasingly high order of accuracy, Journal of Computational Physics 160 (2000) 405–452.
[3] C. Bernardi, Y. Maday, Approximations spectrales de problèmes aux limites elliptiques, in: J.M. Ghidagliaet, P. Lascaux (Eds.), Collection Mathématiques & Applications, Springer, Berlin, 1992.
[4] C. Canuto, M.Y. Hussaini, A. Quarteroni, T.A. Zang, Spectral Methods in Fluid Dynamics, Springer, New York, 1988.
[5] J. Casper, Finite-volume implementation of high-order essentially nonoscillatory schemes in two dimensions, AIAA Journal 30 (1992) 2829–2835.
[6] B. Cockburn, C.W. Shu, The Runge–Kutta discontinuous Galerkin method for conservation laws V, Journal of Computational Physics 141 (1998) 199–224.
[7] V. Daru, C. Tenaud, Evaluation of TVD high resolution schemes for unsteady viscous shocked flows, Computers and Fluids 30 (2001) 89–113.
[8] F. Ducros, V. Ferrand, F. Nicoud, C. Weber, D. Darracq, C. Gacherieu, T. Poinsot, Large Eddy simulation of shock/turbulence interaction, Journal of Computational Physics 152 (1999) 517–549.
[9] A. Harten, B. Engquist, S. Osher, S. Chakravarthy, Uniformly high order essentially non-oscillatory schemes, III, Journal of Computational Physics 71 (1987) 231–303.
[10] G.S. Jiang, C.W. Shu, Efficient implementation of weighted ENO schemes, Journal of Computational Physics 12 (1996) 202–228.
[11] K. Khalfallah, A. Lerat, Correction d'entropie pour des schémas numériques approchant un système hyperbolique', Comptes Rendus à l'Académie des Sciences 308 II (1989) 815–820.

[12] D. Knight, H. Yan, A.G. Panaras, A. Zheltovodov, Advances in CFD prediction of shock wave turbulent boundary layer interactions, Progress in Aerospace Sciences 39 (2003) 121–184.
[13] D. Lax, B. Wendroff, Systems of conservation laws, Communications on Pure and Applied Mathematics 13 (1960) 217–237.
[14] S.K. Lele, Compact finite difference schemes with spectral-like resolution, Journal of Computational Physics 103 (1992) 16–42.
[15] B.P. Leonard, The ULTIMATE conservative difference scheme applied to unsteady one-dimensional advection, Computer Methods in Applied Mechanics and Engineering 88 (1991) 17–74.
[16] M. Lesieur, P. Comte, Large Eddy simulations of compressible turbulent flows, in: Cours AGARD-VKI, Turbulence in Compressible Flows, 1997.
[17] K. Mahesh, A family of high-order finite difference schemes with good spectral resolution, Journal of Computational Physics 145 (1998) 332–358.
[18] R. Peyret, Spectral Methods With Application to Incompressible Viscous Flow, Springer, Berlin, 2002.
[19] C.W. Shu, TVB uniformly high order schemes for conservation laws, Mathematics of Computation 49 (1987) 105–121.
[20] C.W. Shu, S. Osher, Efficient implementation of essentially non-oscillatory shock-capturing schemes, Journal of Computational Physics 77 (1988) 439–471.
[21] C.W. Shu, S. Osher, Efficient implementation of essentially non-oscillatory shock-capturing schemes, II, Journal of Computational Physics 83 (1989) 32–79.
[22] C.W. Shu, T.A. Zang, G. Erlebacher, D. Whitaker, S. Osher, High order ENO schemes applied to two- and three-dimensional compressible flows, Applied Numerical Mathematics: Transactions of IMACS 9 (1992) 45–71.
[23] C.W. Shu, Essentially non-oscillatory and weighted essentially non-oscillatory schemes for hyperbolic conservation laws, NASA/CR-97-206253 and ICASE Report, 1997 pp. 97–65.
[24] B. Sjogreen, H.C. Yee, Grid convergence of high order methods for multiscale complex unsteady viscous compressible flows, Journal of Computational Physics 185 (2003) 1–26.
[25] A. Suresh, H.T. Huynh, Accurate monotonicity-preserving schemes with Runge–Kutta time stepping, Journal of Computational Physics 136 (1997) 83–99.
[26] V.A. Titarev, E.F. Toro, ADER: arbitrary high order Godunov approach, Journal of Scientific Computing 17 (1–4) (2002) 609–618.
[27] C. Tenaud, E. Garnier, P. Sagaut, Evaluation of some high-order shock capturing schemes for direct numerical simulation of unsteady two-dimensional free flows, International Journal for Numerical Methods in Fluids 126 (2000) 202–228.
[28] P. Woodward, P. Collela, The numerical simulation of two-dimensional fluid flow with strong shocks, Journal of Computational Physics 54 (1984) 115–173.